iScience

CellPress
OPEN ACCESS

Article

A porous cervical mucus plug leads to preterm birth induced by experimental vaginal infection in mice

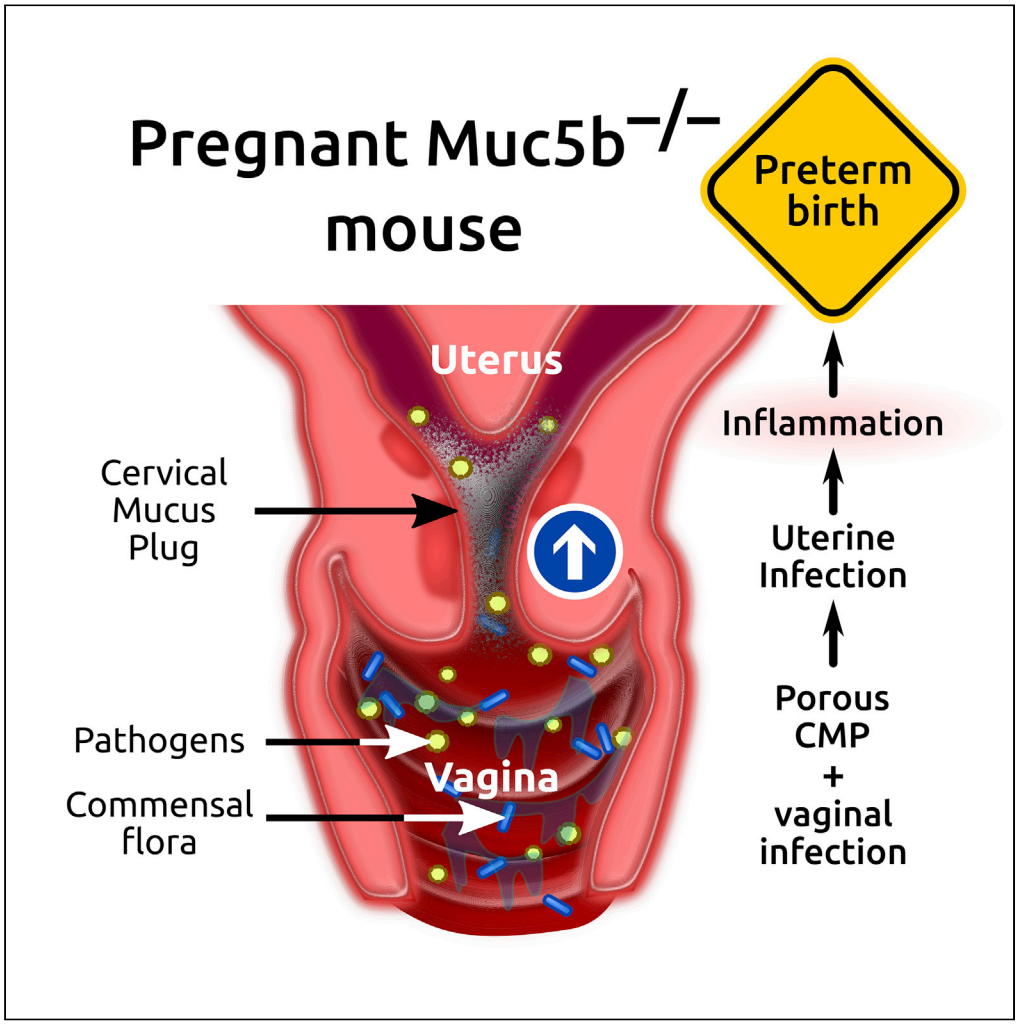

Guillaume Lacroix, Valérie Gouyer, Mylène Rocher, Frédéric Gottrand, Jean-Luc Desseyn

jean-luc.desseyn@inserm.fr

Highlights

Muc5b and Muc5ac are the main gel-forming mucins of the mouse vagina and cervical canal

During pregnancy, a cervical mucus plug (CMP) is formed and seals the cervical canal

Muc5b-deficient CMP is highly porous

Inflammation following vaginal infection causes preterm birth in Muc5b-deficient mice

Lacroix et al., iScience *25*, 104526
July 15, 2022
https://doi.org/10.1016/j.isci.2022.104526

iScience

CellPress
OPEN ACCESS

Article

A porous cervical mucus plug leads to preterm birth induced by experimental vaginal infection in mice

Guillaume Lacroix,[1] Valérie Gouyer,[1] Mylène Rocher,[1] Frédéric Gottrand,[1] and Jean-Luc Desseyn[1,2,*]

SUMMARY

During gestation, the cervical mucus plug (CMP) acts to seal the cervical canal. Pilot studies in humans have suggested that a porous CMP may increase the risk of uterine infection and preterm birth. We examined the gel-forming content of the mouse vagina and the CMP. We experimentally infected pregnant mice by intravaginal administration of pathogens related to preterm birth in humans. We found that the epithelium in both the vagina and cervical canal of pregnant mice produced the two gel-forming mucins Muc5b and Muc5ac. The CMP was porous in Muc5b-deficient mice for which intravaginal administration of *Escherichia coli* O 55 led to the activation of an inflammatory response in the uterus and 100% preterm births. The pathogen was found in the mucus plug and uterus. This study shows that Muc5b is essential for the *in vivo* barrier function and the prevention of uterine infections during gestation.

INTRODUCTION

Preterm birth is associated with significant neonatal morbidity and mortality, and with a higher risk of adverse consequences in childhood and adulthood (Platt, 2014; Ream and Lehwald, 2018; Sperling and Nelson, 2016). Intrauterine infection during pregnancy is recognized as a leading cause (40%) of preterm delivery (Stinson and Payne, 2019). It represents a major obstetric and global health problem that affects more than one in 10 births worldwide (Liu et al., 2015).

During human pregnancy, a large amount of mucus is produced in the cervical canal to form the cervical mucus plug (CMP). It is believed that the CMP acts as a physical barrier that prevents pathogens of the vaginal flora from ascending into the uterine cavity, thereby helping to ensure the sterility of the uterus during pregnancy (Bastholm et al., 2014). A spontaneously expelled CMP in a healthy woman is made of solid-like materials. Mucus is a hydrogel made mainly of water and gel-forming mucins (GFMs), which represent its main organic component and are responsible for its viscoelastic properties (Demouveaux et al., 2018; Lacroix et al., 2020). GFMs are large and heavily *O*-glycosylated proteins that are secreted by specialized cells at the epithelial surface. The secreted long polymers of GFMs form a highly hydrophilic network, which adopts a gel formation when in contact with water. Five GFMs have been identified in humans and named MUC2, MUC5AC, MUC5B, MUC6, and MUC19. These are all highly conserved in mice and named Muc2, Muc5b, Muc5ac, Muc6, and Muc19 (Desseyn and Laine, 2003; Lacroix et al., 2020).

The *in vivo* mucus properties of the CMP are poorly understood because of the difficulties in studying it in humans for ethical and safety reasons. In the human cervical canal, GFMs are secreted by mucus cells located in the endocervical epithelium and form the mucus plug during pregnancy. To date, only three GFMs, MUC2, MUC5AC, and MUC5B, have been detected in the human CMP (Habte et al., 2008). A pilot case–control study reported that the CMP is more extensive and permeable in women at high risk of preterm birth than in those at low risk of preterm birth (Critchfield et al., 2013). In another pilot study, a decrease in mucoadhesive properties of the CMP was observed in women at high risk of preterm birth. These findings suggest that both the microstructural rearrangement of the components of mucus and biochemical modifications to their adhesiveness may alter the overall permeability of the CMP (Smith-Dupont et al., 2017). Taken together, these earlier findings suggest a direct link between a too porous CMP and uterine infection leading to an increased risk of premature birth; however, experimental evidence remains to be provided.

[1]University Lille, Inserm, CHU Lille, U1286 – Infinite, 59000 Lille, France

[2]Lead contact

*Correspondence: jean-luc.desseyn@inserm.fr

https://doi.org/10.1016/j.isci.2022.104526

Animal models may be helpful for studying the structure–function relationship in the CMP by investigating the relationship between experimental vaginal infection and preterm birth. Reproduction studies in domestic animals have described the presence of the CMP in mares, ewes, and cows, which suggests that the production of the CMP is likely conserved in many if not all pregnant mammals (Loux et al., 2017; Owiny et al., 1991). The mouse may represent a valuable mammal model for examining the CMP and its functions because of the ability to use genetically modified strains specific for GFMs. In this study, we used RT-qPCR and imaging to characterize the GFM content in the mouse vagina and CMP. We found that Muc5b and Muc5ac were the two major GFMs and that mucus cells were present in both the vaginal and cervical compartment. Using *in vivo* experiments, we found that Muc5b-deficient CMPs were more porous and led to preterm birth after an experimental vaginal infection. Together, our data support the idea of the crucial protective function of the CMP and its mucin content.

RESULTS

A CMP is formed during pregnancy in mice

Histology using Alcian blue–periodic acid–Schiff (AB–PAS) staining revealed that large amounts of glycoconjugates formed the CMPs that sealed the cervical lumen in wild-type (WT) pregnant mice (Figure 1A). The CMP was surrounded by an epithelium that was also stained strongly with AB–PAS, which suggested that epithelial cells secrete GFMs that participate in the formation of the CMP. The CMP biomaterial appeared to be extremely dense and organized with many parallel layers (Figure 1A). No AB–PAS material was found in the cervical canal of nonpregnant mice (Figure 1B). Immunohistochemistry (IHC) revealed strong staining of both Muc5b and Muc5ac GFMs associated with epithelial cells in the cervical canal of WT pregnant mice (Figure 1C). We did not observe Muc2 or Muc6 in the CMP and cervices of pregnant mice (Figure 1D). At the mRNA level, high expression of *Muc5b* was found, followed by *Muc5ac,* very low expression of *Muc2*, and no expression of *Muc6* Figure 1E).

A dense CMP was also observed using hematoxylin–eosin (HE) and AB–PAS staining in Muc5b-GFP mice (Figure 2A). Both *Ulex europaeus agglutinin* I (UEA1) and *Maackia amurensis agglutinin* (MAA) lectins, which recognize mucin terminal glycotopes fucose α-(1,2)-galactose and α-(2,3)-linked sialic acid, respectively, stained the CMP and epithelial cells in pregnant WT and Muc5b-reporter mice (Figures 2B and 2C) and in pregnant Trefoil factor 3 (Tff3)-reporter mice (Figure 2D). Dual lectin staining highlighted the highly structured CMP with alternating green (UEA1) and red (MAA) and, less clearly, yellow threads or lamellae (Figure 2D).

IHC showed both Muc5b and Muc5ac in the CMP of Muc5b–GFP reporter mice (Figure 3A). The cervical canal exhibited different cell populations that expressed either Muc5b or Muc5ac alone or these two GFMs (Figure 3B).

Light-sheet fluorescence microscopy to access the CMP after the optical clearing protocol was performed in the vagina/cervical canal of a homozygous Muc5b–GFP mouse using UEA1 lectin combined with anti-GFP antibody. The vaginal and cervical canal epithelium were shown to be lined with $Muc5b^{+}$ cells and the upper part of the canal filled with mucus (Video S1, iDISCO dual-labeling of the vaginal fornix and cervical canal of a transgenic reporter Muc5b–GFP pregnant mouse at gestational day 14.5 in the supplemental information).

Muc5b and Muc5ac are the two main GFMs in the mouse vagina

IHC of vaginas revealed that Muc5b and Muc5ac were expressed in the vaginal epithelium, but not Muc2 or Muc6, in WT pregnant mice (Figure 4A). $Muc5b^{+}$ and $Muc5ac^{+}$ biomaterial was found in the vaginal lumen of WT pregnant mice along with epithelial cells that expressed these two GFMs (Figure 4B). These observations were confirmed in Muc5b–GFP pregnant mice. The GFP tag in the reporter Muc5b mouse did not show distinct mucus cell populations for the two GFMs in vaginas (Figure 4C) in contrast to the cervical canal (Figure 3B).

The amount of GFMs produced by vaginal cells varies during the estrus phase

The presence of mucus cells in the vagina of pregnant mice led us to examine the GFM content during the estrus phase in the vagina of nonpregnant mice. Mucus cells were observed only during the diestrus and proestrus phases, and immunofluorescence studies showed that their production of Muc5b and Muc5ac was highest during the diestrus phase (Figure 5).

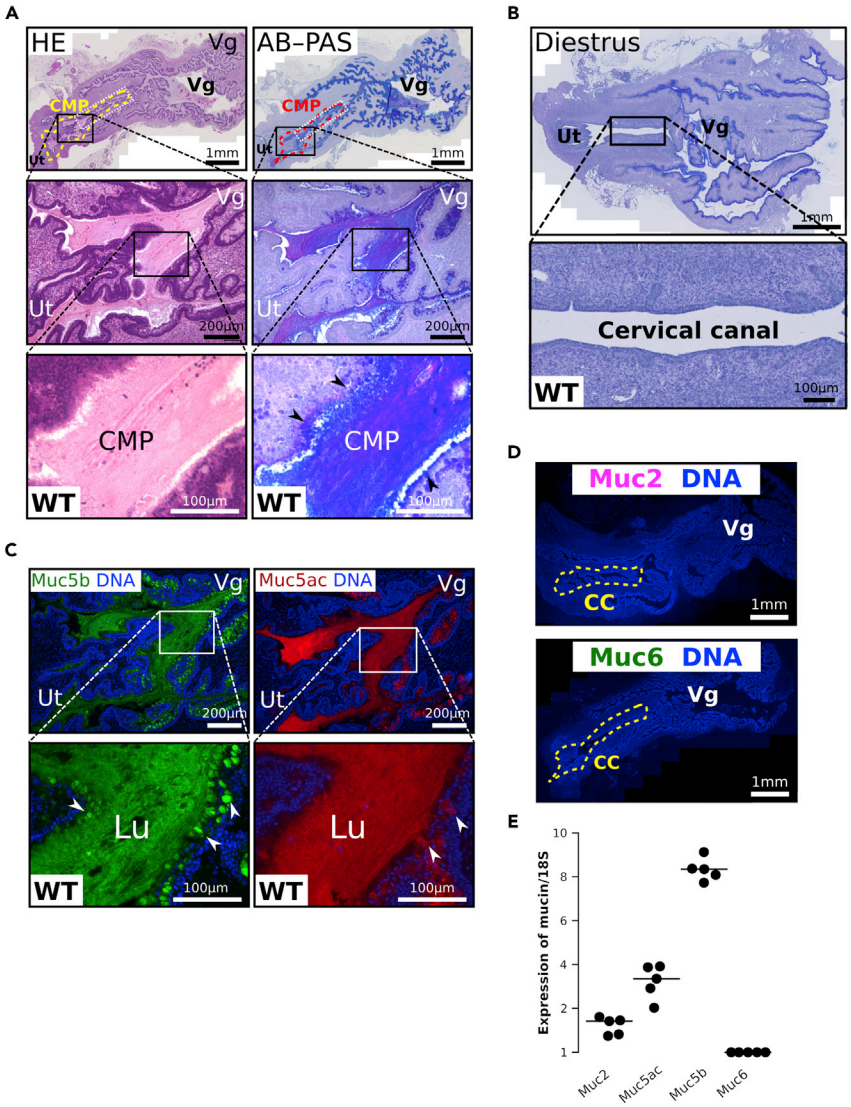

Figure 1. Muc5b and Muc5ac are the two main gel-forming mucins in the mouse CMP

(A) Representative histological images (serial sections) of the cervical mucus plug (CMP) from five wild-type (WT) mice. Arrowheads indicate mucus cells. The white dashes delimit the cervical canal. HE, hematoxylin–eosin; AB–PAS, Alcian blue–periodic acid–Schiff.

(B) Longitudinal sections of the genital tract stained with AB–PAS from a nonpregnant WT mouse during diestrus showing the absence of AB–PAS^{+} biomaterial in the cervical canal compared with pregnant mice (A). Similar images showing the absence of AB–PAS^{+} material were observed during other phases of the cycle (not shown).

(C) Immunofluorescence analysis of Muc5b (green) and Muc5ac (red) in serial sections of the CMP and vagina (Vg). The images are representative of five WT mice. Arrowheads outline mucus cells.

(D) No Muc2 or Muc6 was observed in wide-field immunofluorescence images of the complex of the Vg and cervical canal (CC) captured using an Axio Scan in pregnant WT mice. DNA was counterstained with Hoechst 33258 dye (blue). Lu, lumen; Ut, uterus.

(E) Expression of gel-forming mucins in the vaginas/cervices of pregnant WT pregnant mice. Results were obtained using the $2^{-\Delta\Delta Ct}$ method.

Tff3 is secreted into the CMP but is not discharged into the vagina

After we found that the mouse vaginal epithelium produces GFMs, we examined whether discharge of the mucus from the CMP may contribute to vaginal mucus in mice as it does in humans. Given that high amounts of TFF3 have been reported in the human CMP (Bastholm et al., 2017), we first confirmed by IHC that mouse Tff3 was also secreted into the mouse CMP (Figure 6A). We then used the Tg222 transgenic

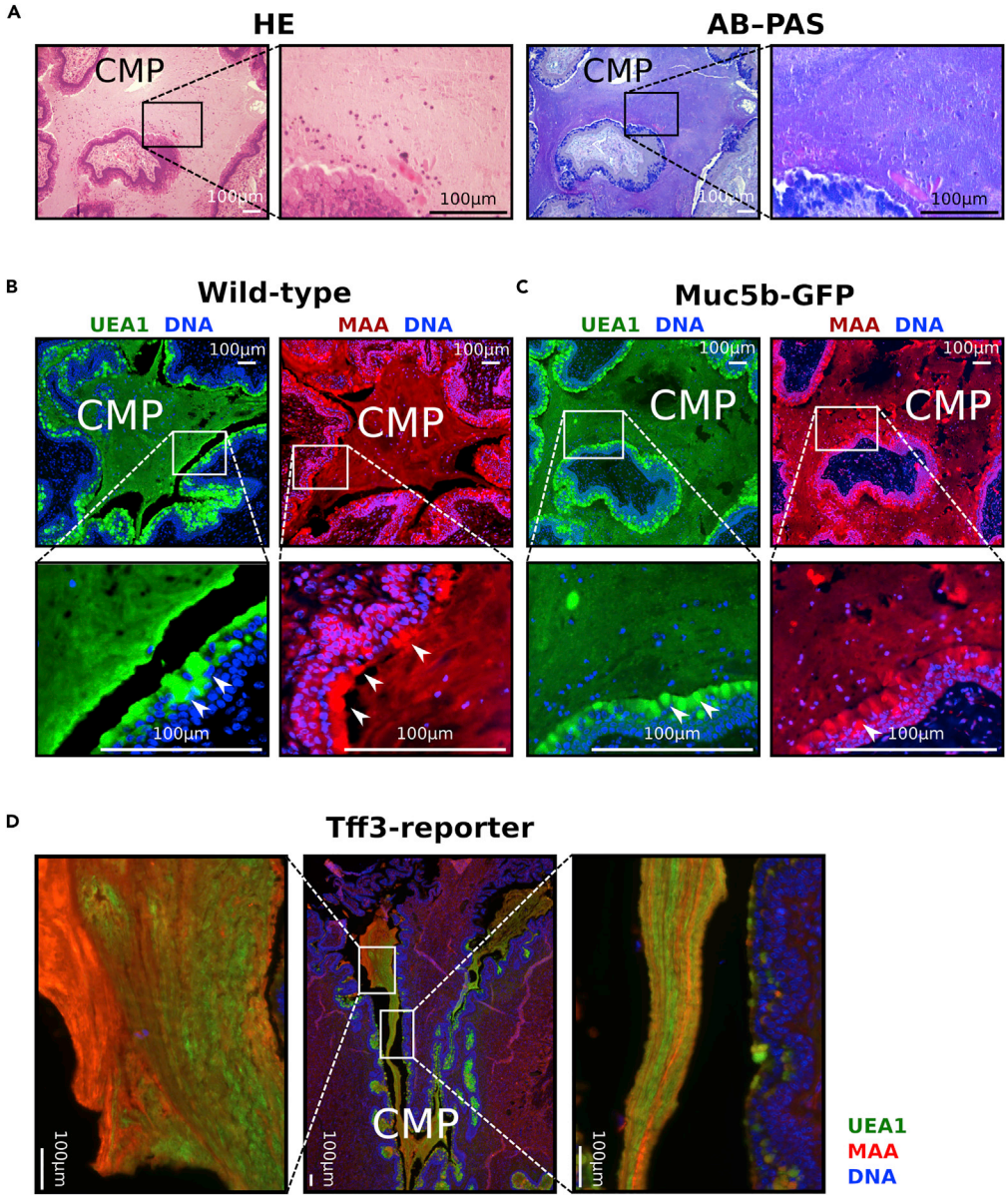

Figure 2. Lectin staining of the CMP in wild-type, Muc5b–GFP, and Tff3 reporter mice

(A) Histology images of the cervical mucus plug (CMP) from Muc5b–GFP mice stained with hematoxylin–eosin (HE) and Alcian blue–periodic acid–Schiff (AB–PAS).

(B–D) Immunofluorescence analysis using *Ulex europaeus agglutinin* I (UEA1) and *Maackia amurensis agglutinin* (MAA) lectins in CMP from wild-type, Muc5b–GFP, and reporter Tff3 (Tg222) mice. Images are representative of three mice/group and should be compared with those in Figure 1. Arrowheads indicate mucus cells.

mouse as a reporter, in which the GFP-tagged transgene is driven by the mouse *Tff3* gene promoter (Gouyer et al., 2015). IHC showed no transgene product in the vagina (Figure 6B) or the cervical canal in nonpregnant mice (not shown) but that Muc5b and the Tg222 transgene product colocalized in the cervical canal of pregnant mice (Figure 6B). The apparent lack of discharge of cervical Tff3 into the vagina suggests that the contribution of GFMs of the CMP to vaginal mucus must be minor.

The CMP of Muc5b$^{-/-}$ mice is porous

The absence of Muc5b in the CMP of Muc5b$^{-/-}$ mice was checked by IHC using both a specific antibody directed against this mucin (Figure 7A) or against the GFP tag of reporter Muc5b (data not shown). We next

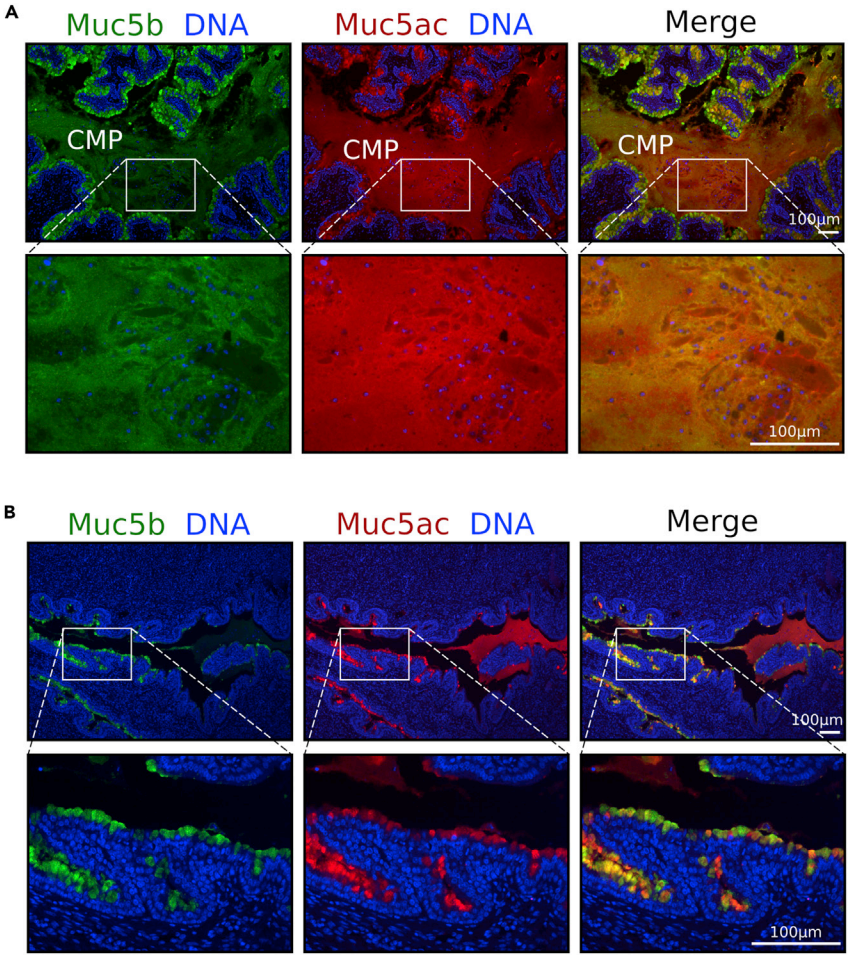

Figure 3. Expression patterns of Muc5b and Muc5ac in the female genital tract from pregnant reporter Muc5b–GFP mice

(A and B) Dual-fluorescence labeling of Muc5b (anti-GFP antibody, green) and Muc5ac (red) of (A) the cervical mucus plug (CMP) and (B) the cervical canal showing cells expressing either Muc5b or Muc5ac or both mucins. Wide-field images were acquired using an Axio Scan and are representative of three mice. DNA was counterstained with Hoechst 33258 dye (blue).

looked by RT-qPCR for a possible compensatory effect of GFMs in Muc5b-deficient mice using mRNA extracted from the complex vagina/cervical canal of pregnant mice. No expression of *Muc6* was found in both WT and Muc5b$^{-/-}$ mice (not shown), whereas expression of *Muc5ac* and *Muc2* expression did not differ between WT and Muc5b$^{-/-}$ mice (Figure 7B). HE staining showed that the cervical canal was almost devoid of materials in Muc5b$^{-/-}$ pregnant mice. This was confirmed by the low AB–PAS staining of cervical canal and mucous cells (Figure 7C). We also studied CMPs of Muc5b$^{-/-}$ mice using lectin staining (Figure 7D). Results were in agreement with a modified CMP in Muc5b-deficient mice observed by HE and AB-PAS and support an absence of compensatory effect by other GFMs in Muc5b$^{-/-}$ mice. Furthermore, we observed a clear staining of mucus cell content of the CMP with UEA1 but a weak staining with MAA that localized only at the cell surface compared to WT mice (see Figure 2B). These observations confirmed that the mucus plug is less dense in Muc5b$^{-/-}$ mice.

No cervical or vaginal damage was observed in pregnant Muc5b$^{-/-}$ mice when using the transcription factor C/EBP homologous protein (CHOP) by RT-qPCR to evaluate ER stress, proliferating cell nuclear antigen (PCNA) to study the rate of cell division (Figures 8A and 8B) and Terminal Deoxynucleotidyl Transferase-Mediated dUTP Nick-End Labeling (TUNEL) for DNA break analysis (data not shown). The vaginal mucosal epithelium (ME)—defined as the terminally differentiated epithelium with visible mucus-laden

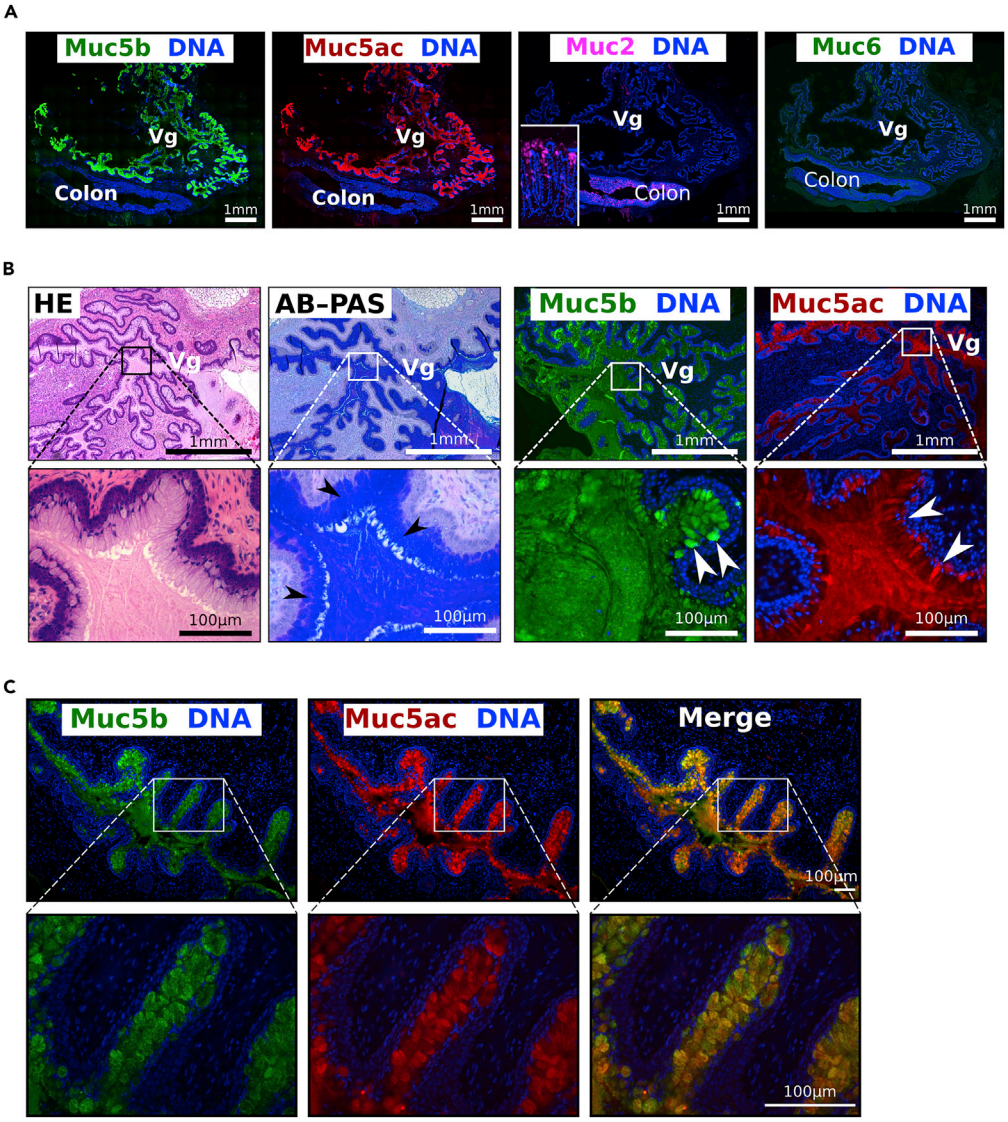

Figure 4. GFMs in the cervix and vagina of pregnant mice

(A) Wide-field immunofluorescence images of serial sections of the vagina (Vg) acquired using an Axio Scan showing Muc5b (green) and Muc5ac (red) in the vaginal epithelium and lumen. Images are representative of five WT mice. Muc2 and Muc6 were not observed in the vaginal epithelium and lumen, but Muc2 was observed in epithelial cells of the colon (zoom-in).

(B) Serial sections stained with hematoxylin–eosin (HE) and Alcian blue–periodic acid–Schiff (AB–PAS) of the Vg and immunofluorescence images of Muc5b (green) and Muc5ac (red). Arrowheads indicate mucus cells. Images are representative of five WT mice.

(C) Dual immunofluorescence images of serial sections of Vg showing Muc5b (GFP, green) and Muc5ac (red) in the vaginal epithelium. The images are representative of three Muc5b-GFP mice. DNA was counterstained with Hoechst 33258 dye (blue) in all immunofluorescent sections.

vacuoles—was depleted in mucous cells and was thinner in Muc5b$^{-/-}$ than in WT mice; this reflected a lower number of AB–PAS^{+} epithelial cells in Muc5b$^{-/-}$ mice (Figure 8C).

The porosity percentage was then determined by image analysis of AB–PAS images using ImageJ (Figure 9A). The CMP was 12.3-fold more porous in Muc5b$^{-/-}$than in WT mice (Figure 9B).

Scanning electron microscopy (SEM) was used to image native cervical mucus from four WT and four Muc5b$^{-/-}$ pregnant mice (Figure 10). The CMP was smaller and more difficult to find in Muc5b$^{-/-}$ mice

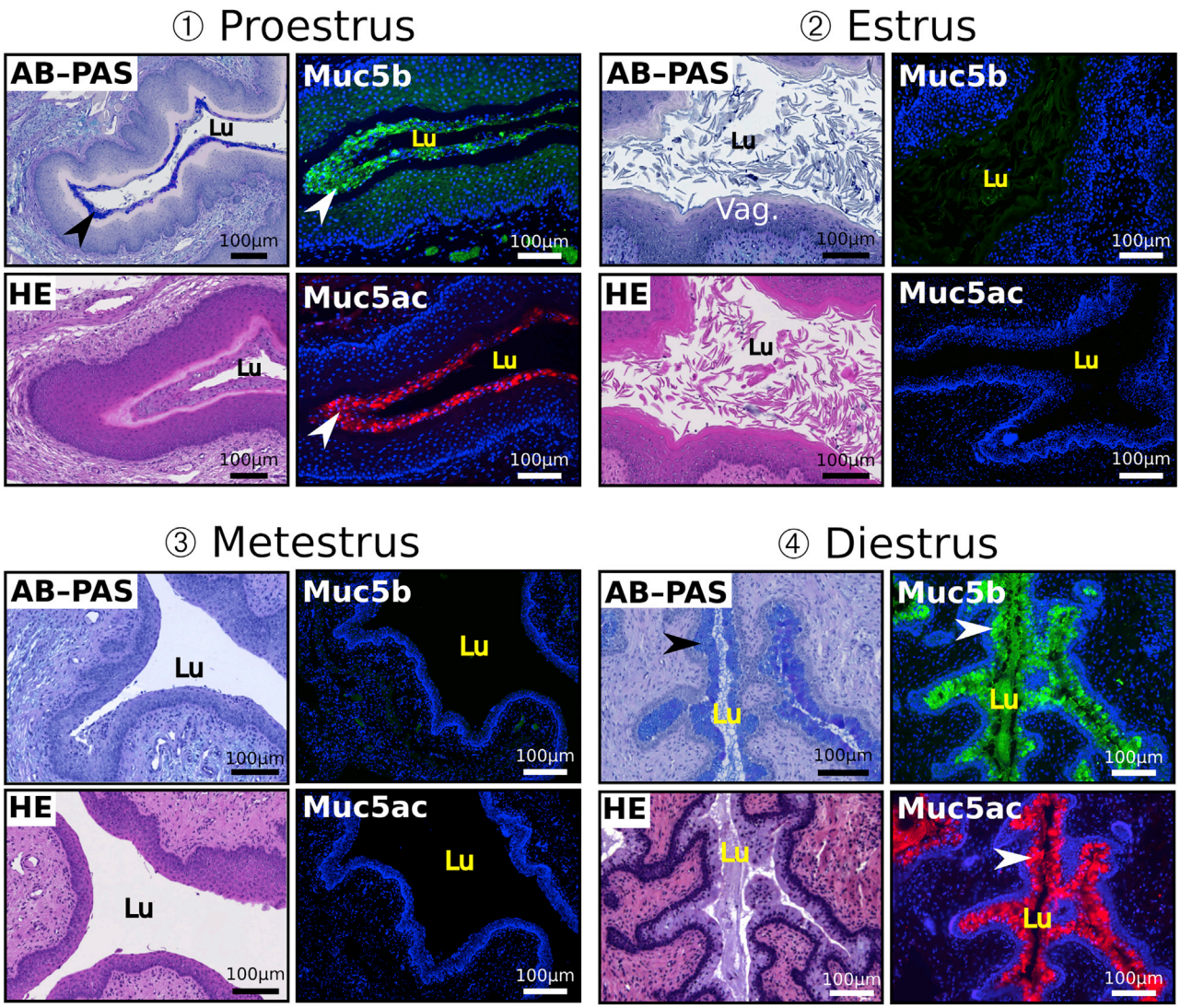

Figure 5. GFMs in the vagina of nonpregnant adult wild-type mice

Vaginas were studied by histology using hematoxylin–eosin (HE) and Alcian blue–periodic acid–Schiff (AB–PAS) and immunofluorescence for the two main gel-forming mucins Muc5b (green) and Muc5ac (red) during the four estrus phases. DNA was counterstained with Hoechst 33258 dye (blue) in all immunofluorescent sections. Images are representative of two to four mice/phase. During diestrus and proestrus, the vaginal epithelium harbored mucus cells (arrowheads) that expressed Muc5b and Muc5ac. Mucin production was higher during the diestrus phase. No AB–PAS^{+} cells, Muc5b, or Muc5ac were observed during estrus and metestrus. Cornified cells were evident in the lumen during estrus. Lu, Lumen.

than in WT mice. The CMP exhibited both parallel and crossing fibers for the two genotypes. However, the ultrastructure of the CMP appeared to be denser and with smaller diameter pores in WT mice. The heterogeneity in the spatial arrangement of the fibers within each sample made it impossible to quantify the pore size; however, small spherical objects were observed in three of the four Muc5b$^{-/-}$ mice examined but never in the 4 WT mice investigated.

Pathogens can pass through the porous CMP to induce preterm birth

To test whether pregnant Muc5b$^{-/-}$ mice may be more susceptible to give birth before term because of their porous CMP, we mimicked vaginal dysbiosis by intravaginal administration at gestational day (GD) 14.5 with vaginal bacteria associated with human preterm birth (Figure 11A). We first tried 10^7 colony-forming units (CFUs) of *Gardnerella vaginalis*. Because no WT and Muc5b$^{-/-}$ mice gave birth before term (Figure 11B), we then challenged mice with *Escherichia coli* O 55. After a pilot study to determine the optimal dose of bacteria, we administered 10^6 CFU per mouse. None of the 10 WT mice gave birth before term,

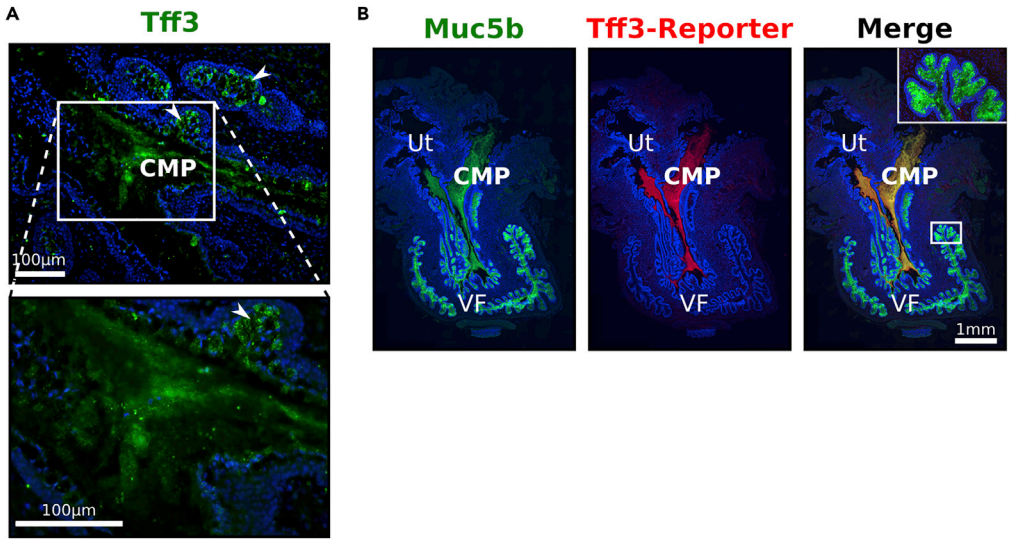

Figure 6. The CMP mucus does not discharge in the vagina

(A) Immunofluorescence images representative of n = 3 wild-type mice showing Tff3 (green) produced in the epithelium of the cervical canal and found in the cervical mucus plug (CMP). Arrowheads outline $Tff3^{+}$ cells.

(B) Wide-field immunofluorescence images representative of n = 3 transgenic Tg222 mice acquired using Axio Scan and showing Muc5b (green) in both the CMP and vaginal fornix (VF), whereas the transgene product (red) of Tff3-reporter mice was found only in the CMP. DNA was counterstained with Hoechst 33258 dye (blue). Ut, Uterus.

whereas all $Muc5b^{-/-}$ mice delivered before term (Figure 11B). No preterm birth resulted after administration of 5×10^6 CFU heat-killed *E. coli* O 55 in $Muc5b^{-/-}$ mice. In all experiments, no preterm living pup was found. We next infected mice with 10^6 CFU *E. coli* O 55 and killed mice before preterm delivery at GD15.5, and used immunofluorescence to try to identify *E. coli* in the vagina, CMP, and uterine cavity. Hoechst 33258 staining suggested cell infiltration in vagina of all mice but in the CMP and uterus of only $Muc5b^{-/-}$ mice (Figure 11C). *E. coli* was found in the vagina of both WT and $Muc5b^{-/-}$ mice. However, *E. coli* was found in the CMP and uterus of $Muc5b^{-/-}$ mice but not of WT mice (Figures 11C and 11D). This finding suggests vaginal pathogens can ascend toward the uterus through the Muc5b-deficient CMP.

Cervical and uterine infection triggers inflammation in $Muc5b^{-/-}$ pregnant mice

As expected, histological examination of mice killed 24 h after intravaginal administration of *E. coli* O 55 showed immune cell infiltration, most likely of neutrophils, in the vagina of all WT and $Muc5b^{-/-}$ mice examined. Massive immune cell infiltration was observed in the CMP of the three $Muc5b^{-/-}$ but not of the three WT mice as illustrated in Figure 12A. Proinflammatory levels of the cytokines CXCL1/keratinocytes-derived chemokine (KC), interleukin 1β (Il-1β), Il-6, and tumor necrosis factor alpha (Tnf-α) in both the total serum and uterine tissue biopsies of the tissue facing the cervical canal of WT and $Muc5b^{-/-}$ mice were measured by enzyme-linked immunosorbent assays (ELISA). Il-1β, Il-6, Il-10, and Tnf-α were not detectable in serum (data not shown). The CXCL1/KC level was higher in the serum of $Muc5b^{-/-}$ than in WT mice (Figure 12B). In uterine tissue, Il-10 and Tnf-α were not detectable (data not shown) but significantly higher Il-1β and Il-6 levels and a trend toward increased CXCL1/KC level were found in $Muc5b^{-/-}$ mice compared with WT mice (Figure 12C). These data suggest that the experimental vaginal infection with *E. coli* O 55 induced a local inflammatory response in the uterus of $Muc5b^{-/-}$ mice correlated with premature labor.

DISCUSSION

The most common pathway to uterine infection during pregnancy is the ascending vaginal route, as demonstrated in pregnant mice using bioluminescent *E. coli* (Stinson and Payne, 2019; Suff et al., 2018). In this context, CMP integrity seems to be critical. Pilot studies have suggested that a porous CMP increases the risk of preterm birth in women (Critchfield et al., 2013; Smith-Dupont et al., 2017), but this has never been demonstrated. Studies have almost always examined the CMP ejected just before delivery or mucus samples of the distal plug compartment or from cervical discharge (for examples, see (Bastholm

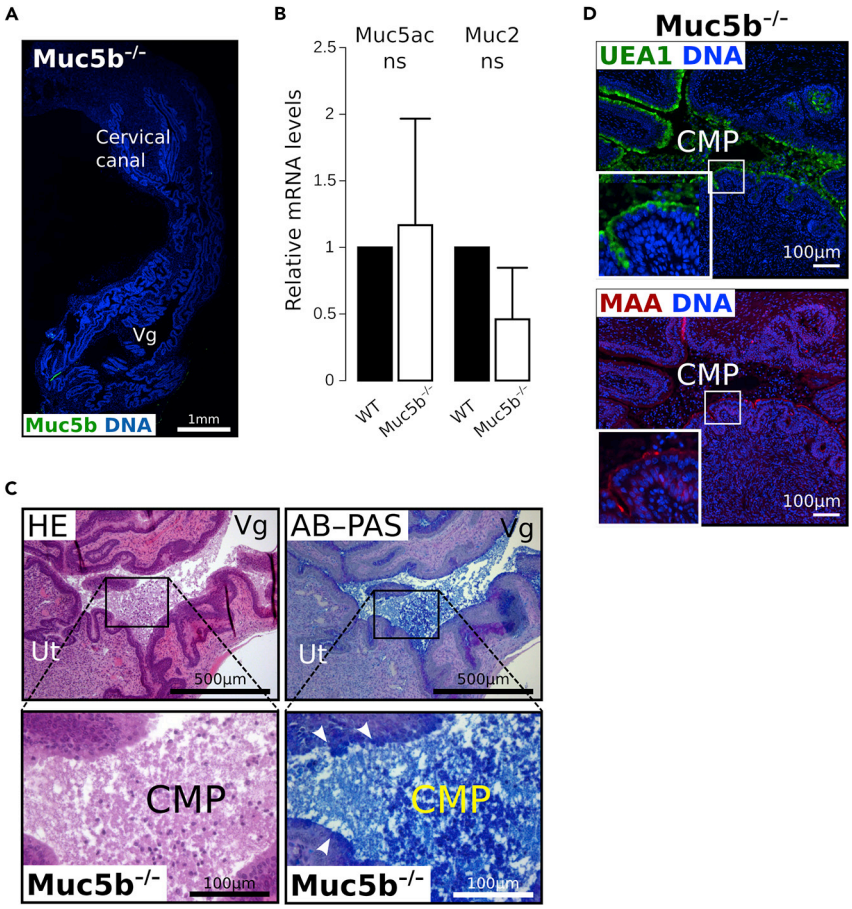

Figure 7. The CMP of Muc5b-deficient mice appears very sparse

(A) Wide-field immunofluorescence images acquired using an Axio Scan showing the absence of Muc5b (green) in the cervical mucus plug (CMP) and vagina (Vg) in Muc5b$^{-/-}$ mice.

(B) Relative *Muc5ac* and *Muc2* expression in vagina/cervix from five wild-type (WT) and five Muc5b$^{-/-}$ pregnant mice. There is no compensatory effect observed by the two mucins. Statistical analysis was conducted using a two-sided Wilcoxon-Mann-Whitney test. Data are represented as mean ± SD. ns, nonsignificant.

(C) Histologically representative images of the CMP from five Muc5b$^{-/-}$ mice. Arrowheads outline the fewer mucus cells compared with WT mice. Vg, vagina; Ut, uterus.

(D) Immunofluorescence analysis using *Ulex europaeus agglutinin* I (UEA1) and *Maackia amurensis agglutinin* (MAA) lectins in the CMP of Muc5b$^{-/-}$ mice showing a weak MAA staining in the CMP. Images are representative of three mice. DNA was counterstained with Hoechst 33258 dye (blue).

et al., 2017, 2014; Critchfield et al., 2013; Hein et al., 2005; Lee et al., 2011; Smith-Dupont et al., 2017)). In nonhuman mammals, the CMP has not been studied thoroughly. Our studies using histology and IHC show that the CMP does exist in mice and that the cervical canal of pregnant mice also secretes GFMs, contrary to what is generally accepted (Sugiyama et al., 2021). To our knowledge, only one study has reported on AB–PAS-stained material in the cervical canal of pregnant mice (Pavlidis et al., 2020) but that observation has not been investigated further. Visualization of the CMP with lectins reveals a very dense structure consisting of alternating layers running from the uterus to the cervix. This multilayered structure is reminiscent of that observed in the gastrointestinal mucus (Gouyer et al., 2011; Matsuo et al., 1997). The extremely tight structure in the CMP we observed by histology and IHC is probably necessary to ensure a perfect seal of the cervical canal.

After several trials, we succeeded in imaging the mouse CMP in 3D using iDISCO and light-sheet microscopy. To our knowledge, this is the first application of this method to acquire spatially resolved imaging of a mucus gel inside the lumen of its native tissue. Unfortunately, the cervix appeared to be open in its proximal part toward the vagina, and the absence of mucus in this same region suggested that part of

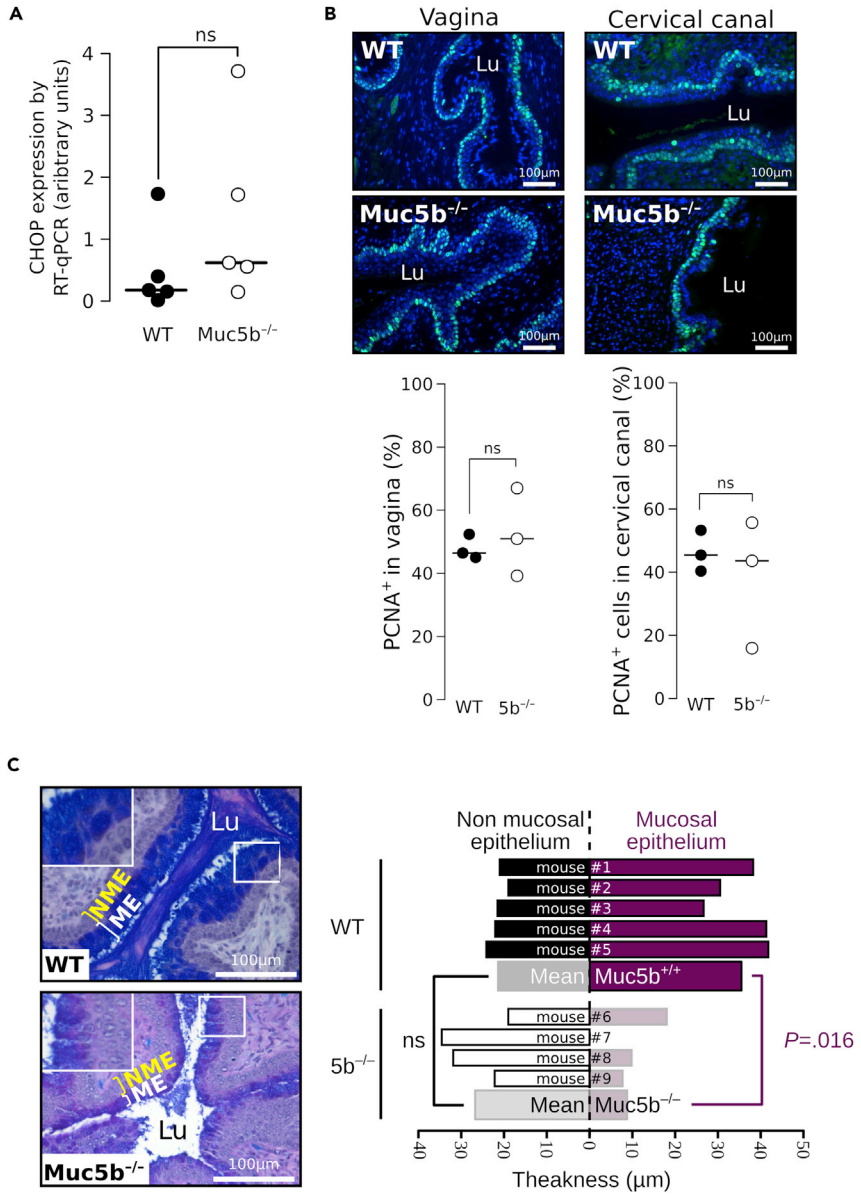

Figure 8. Integrity of the genital epithelium in Muc5b$^{-/-}$ pregnant mice

(A) Expression of CHOP assessed by RT-qPCR in the vagina and cervix from five wild-type (WT) and five Muc5b$^{-/-}$ mice.

(B) Immunofluorescence images of proliferating cell nuclear antigen (PCNA, in green) of three representative WT and three Muc5b$^{-/-}$ (5b$^{-/-}$) mice. The percentages of PCNA^{+} cells relative to total epithelial cells were determined in the vagina and cervical canal for three mice/genotype.

(C) Histology sections stained with Alcian blue–periodic acid–Schiff showing the decrease in thickness of the vaginal mucosal epithelium (ME). The thickness of the nonmucosal epithelium (NME) and ME was measured in five WT and four Muc5b$^{-/-}$ mice. Lu, lumen. DNA was counterstained with Hoechst 33258 dye (blue) in all immunofluorescence sections. Statistical analysis was conducted using a two-sided Wilcoxon-Mann-Whitney test. ns, non-significant.

the CMP was probably lost during the different steps of the sample preparation. In addition, the iDISCO protocol produces significant shrinkage of the tissue by up to 50% of its volume (Velíšek, 2016), which likely reflects loss of its watery mucus content and highlights the need for improving the protocol to ensure better preservation of the tissue structure and its mucus gel.

We found that the mucin content of the mouse CMP is similar to that in humans in that both contain the two main GFMs Muc5b and Muc5ac, a finding that agrees with previous results in humans and rhesus macaques

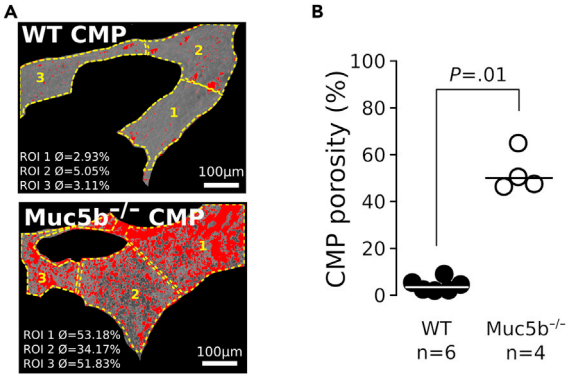

Figure 9. The Muc5b$^{-/-}$ CMP is porous

(A) Illustration showing the image processing using ImageJ. CMP porosity was determined as the mean of the porosity from three distinct regions of interest (ROIs) per CMP from wild-type (WT) and Muc5b$^{-/-}$ mice.

(B) CMP porosity as a percentage in six WT and four Muc5b$^{-/-}$ mice. Statistical analysis was conducted using a two-sided Wilcoxon-Mann-Whitney test.

(Habte et al., 2008; Han et al., 2021; Lee et al., 2011; Wickstrom et al., 1998). Unexpectedly, our histology and IHC studies highlighted major differences between the human and the mouse. We found that the Tff3 peptide was secreted into the cervical canal, which is consistent with the suggestion that TFF3 plays a role in the viscoelastic properties of the CMP in humans (Bastholm et al., 2017). However, it has been reported a strong staining for TFF3 of submucosal glands in the human vagina (Madsen et al., 2007). We did not observe the Tff3 in the vagina during pregnancy and in nonpregnant mice, except a very weak expression during proestrus (not shown). In women, vaginal mucus originates from discharge of cervical mucus, as shown in a study that used Northern blot analysis, *in situ* hybridization, and IHC that found an absence of GFMs in both the ectocervix and vagina (Gipson et al., 1997). By contrast, in the mouse, the two GFMs Muc5b and Muc5ac are secreted by the cervical epithelium during pregnancy, as expected, but the vagina secretes these GFMs during both pregnancy and at times in the estrus cycle.

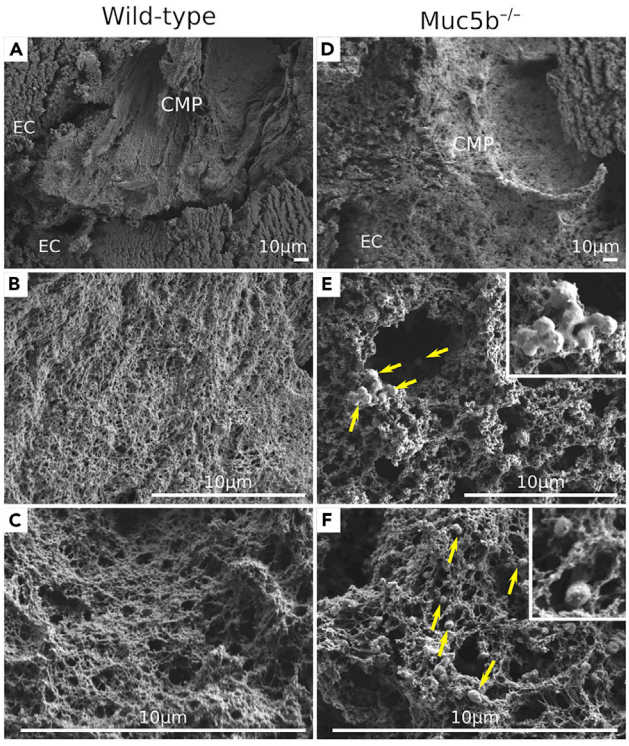

Figure 10. Ultrastructure of the cervical mucus plug

Representative photographs of the cervical mucus plug (CMP) from four wild-type (a–c) and four Muc5b$^{-/-}$ (d–e) pregnant mice by scanning electron microscopy. The images in (e) and (f) are of two different CMPs. Arrows indicate the round objects are potentially bacteria. Cluster of microbial cells enclosed in an extracellular polymeric substance matrix (f) that is characteristic of a bacterial biofilm. EC, epithelial cell.

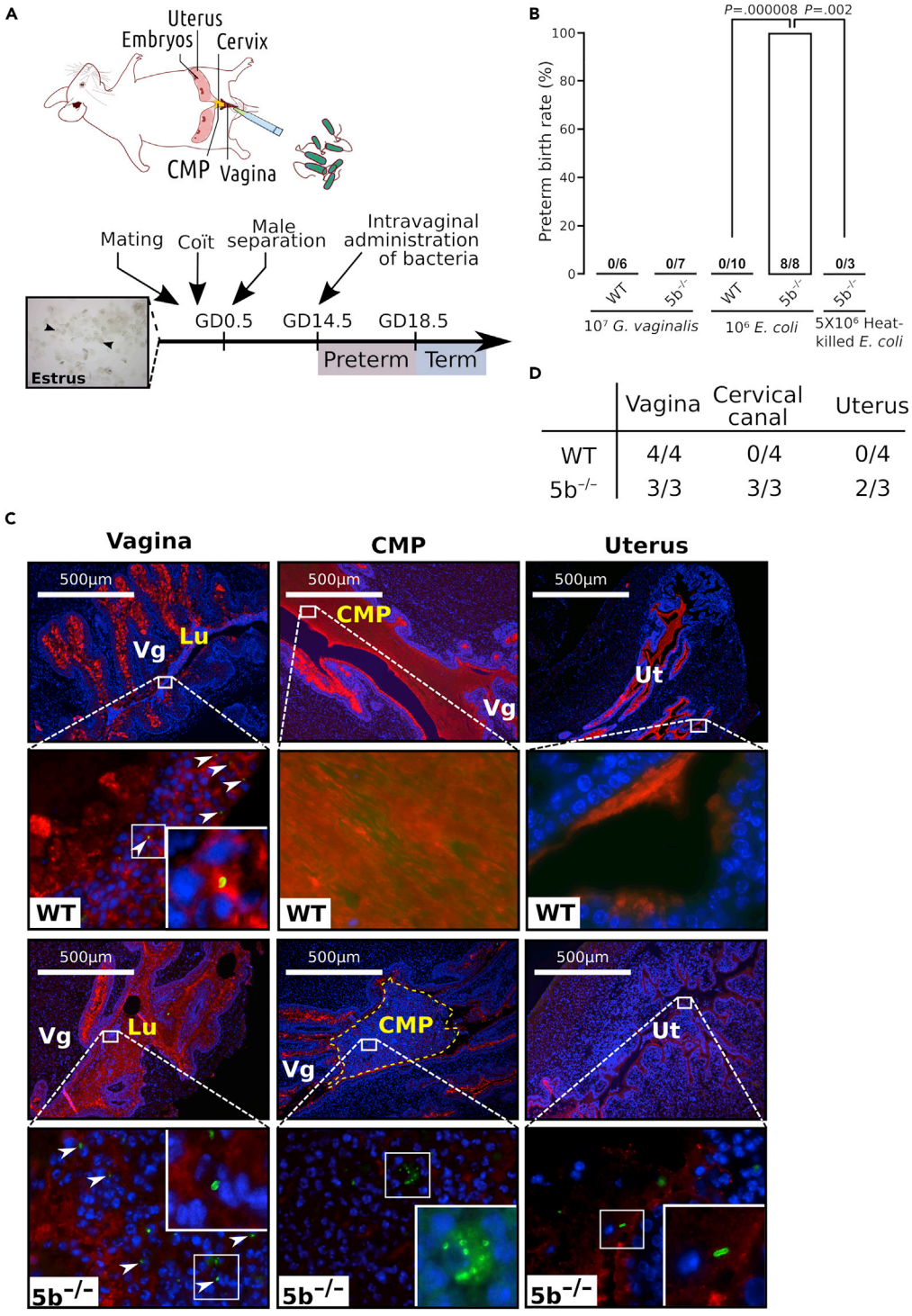

Figure 11. *E. coli* ascent toward the uterus in Muc5b$^{-/-}$ pregnant mice associated with preterm birth

(A) Study design. Female mice in the estrus phase, identified using vaginal smears, showing cornified epithelial cells (arrowheads) were mated for one night with one male. Pregnant mice were infected intravaginally at gestational day (GD) 14.5 with either *G. vaginalis or E. coli* O 55. Delivery before GD18.5 was considered as preterm birth.

(B) Preterm frequency in wild-type (WT) and Muc5b$^{-/-}$ (5b$^{-/-}$) mice. Data were analyzed using the nonparametric Barnard's test. The number (n) of mice/group is depicted.

Figure 11. *Continued*

(C) *E. coli* (green) were observed by immunofluorescence in vagina of WT and Muc5b$^{-/-}$ mice (arrowheads) and in the cervical mucus plug (CMP) and uterus (Ut) of Muc5b$^{-/-}$ but not of WT mice 24 h after intravaginal administration. Wide-field images were acquired using an Axio Scan (n = 3 mice/group). Mucus was stained using *Ulex europaeus agglutinin* I (UEA1) lectin (red) and counterstained for DNA with Hoechst 33258 dye (blue) showing massive cell infiltration in the vagina of both WT and Muc5b$^{-/-}$ mice and in the CMP of Muc5b$^{-/-}$ but not WT mice. Vg, vagina.

(D) Frequency of *E. coli* O 55 found in the cervical canal and uterus of infected pregnant mice (n = 4 WT and n = 3 Muc5b$^{-/-}$).

IHC did not show this flow of mucus from the cervical canal toward the vagina using our reporter Tff3 mouse. This may deserve further investigations. The content of mucus and Muc5b varied during the mouse estrus cycle, and the peak of Muc5b occurred during diestrus, which suggests hormonal regulation, as reported in studies of women showing that the MUC5B content in cervical mucus peaks at midcycle (Gipson et al., 2001).

Muc5b$^{-/-}$ mice proved to be an excellent tool for testing the hypothesis that a porous CMP leads to a higher risk of preterm birth. Our histology and IHC findings showed that the absence of Muc5b was related to a highly porous CMP. We successfully imaged the mouse CMP using SEM. Several groups have studied the ultrastructure of human cervical mucus; but to our knowledge, the CMP has not been imaged *in situ*. The high water content of the mucus gel, heterogeneity in the spatial arrangement of mucin fibers within each CMP, and sample preparation steps that likely altered the CMP structure, make ultrastructural studies of the CMP by SEM difficult. However, we found clear modifications of the CMP ultrastructure in Muc5b$^{-/-}$ compared with WT pregnant mice. SEM revealed objects that were observed only in Muc5b-deficient CMPs, and the round shape and small size of these objects are compatible with the presence of cocci. The presence of these objects in the CMP of Muc5b$^{-/-}$ but not in WT mice is consistent with a porous CMP in Muc5b-deficient mice. Using lectins, control and Muc5b-deficient CMPs support that UEA1 stains with Muc5ac, whereas MAA stains with Muc5b in agreement with our previous observations in the mouse nose and with studies from others in mouse and pig airways that showed co-localization of Muc5ac/MUC5AC with UEA1 and Muc5b/MUC5B with MAA lectins (Amini et al., 2019; Dickinson et al., 2019; Ermund et al., 2017).

Our Muc5b$^{-/-}$ mice are viable and fertile, and we have not observed any preterm birth in our animal facility after at least 10 generations. Our study did not note any damage to the vaginal or cervical epithelium in unchallenged Muc5b$^{-/-}$ mice but only a thinner vaginal epithelium. Several bacterial challenges have been reported to induce preterm birth in mice. We first used *G. vaginalis*, because this bacterium is a common vaginal pathogen in women with vaginal dysbiosis and is frequently found in pregnant women with intra-amniotic infection (Mendz et al., 2013; Muzny et al., 2019). Although this pathogen is linked to preterm labor, the virulence of the bacterium is strain-dependent and the induced preterm birth rate was 0–20% in studies of WT CD-1 mice (McDonald et al., 1991; Muzny et al., 2019; Sierra et al., 2018). In our hands, a single vaginal administration of *G. vaginalis* at GD14.5 or two administrations at GD14.5 and GD15.5 did not induce preterm labor in Muc5b$^{-/-}$ mice with the C57BL/6 background.

We identified *E. coli* O 55 as a good candidate to test our hypothesis. This pathogenic enterobacterium is frequently associated with intra-amniotic infection, and its colonization of the vagina and urinary tract is linked to increased preterm labor and poor pregnancy outcomes (McDonald et al., 1991; Mendz et al., 2013; Migale et al., 2015). We successfully induced preterm birth for all Muc5b$^{-/-}$ mice by intravaginal administration of the pathogen *E. coli* O 55 but not using heat-killed bacteria. In addition, none of the pregnant WT mice infected with living *E. coli* O 55 had a preterm birth. *E. coli* O 55 was found in the CMP and uterine cavity of Muc5b$^{-/-}$ mice, although we cannot exclude the possibility that bacteria from the vaginal commensal flora also ascended into the uterine cavity.

Both immune cell infiltration and an increased proinflammatory response were observed only in Muc5b$^{-/-}$ pregnant mice but not in WT pregnant mice. The levels of cytokines in infected pregnant mice were often very low or were not detectable, and there was great heterogeneity in the concentration of cytokines in Muc5b$^{-/-}$ mice (Figures 12B and 12C). This heterogeneity most likely reflects the resolution of the inflammation, which was highly variable between mice. The heterogeneity may also have been partly a function of the timing of the onset of inflammation and the time lapse, which can be as long as 15 h, between the premature nocturnal delivery and the collection of serum and tissues the following morning. According to

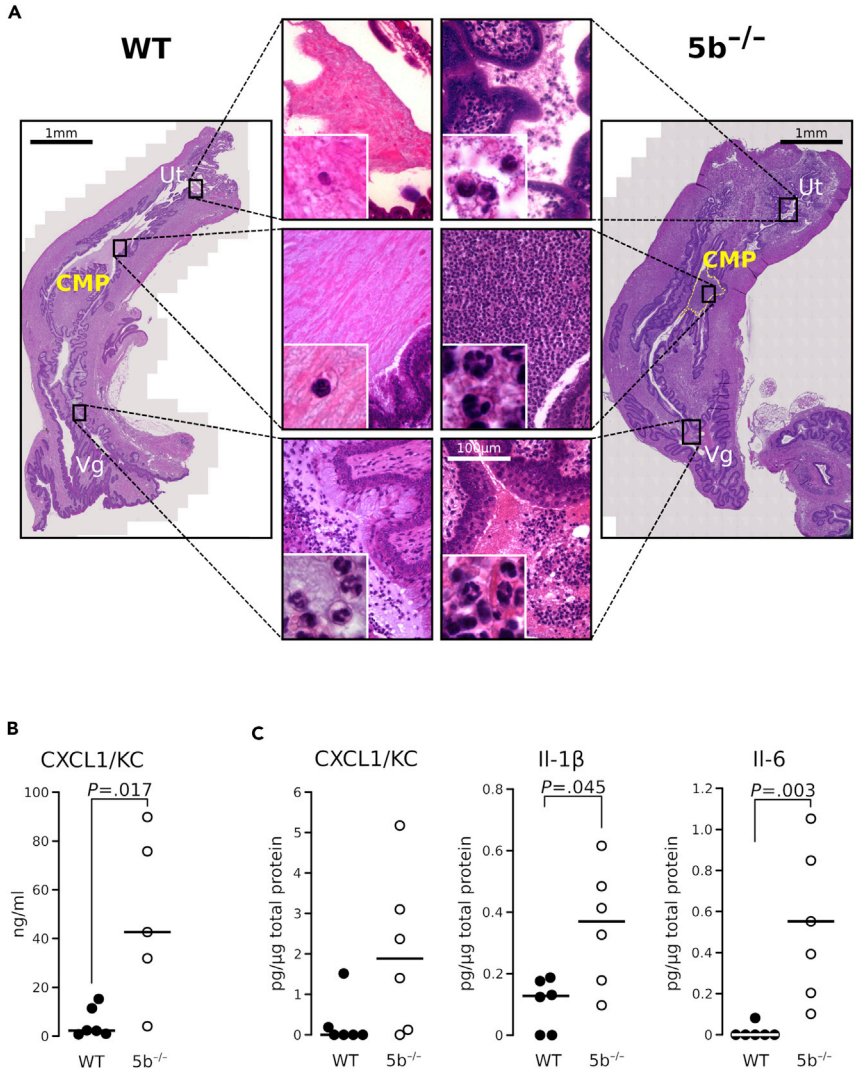

Figure 12. Intravaginal administration of *E. coli* triggers cervical and uterine inflammation in Muc5b-deficient mice

(A) Wide-field images of sections stained with hematoxylin–eosin. Images were acquired using an Axio Scan and show massive neutrophilic cell infiltration in the CMP, vagina, and uterus of Muc5b$^{-/-}$ mice but not WT mice 24 h after intravaginal administration *of E. coli* O 55. Images are representative of n = 3 mice/genotype.

(B and C) Level of CXCL1/KC determined by ELISA in serum and (C) CXCL1/KC, Il-6, and Il-1β in uterine tissue collected within 15 h of birth (n = five to six mice/group). Statistical analysis was conducted using a two-sided Wilcoxon-Mann-Whitney test.

Migale et al., once in the intrauterine cavity, lipopolysaccharide from *E. coli*, including the O55:B5 strain we used, activates uterine inflammatory pathways and increases the production of proinflammatory cytokines including the key inflammatory mediator IL-1β, which result in spontaneous myometrium contractions leading to preterm birth (Migale et al., 2015).

Our work provides the first characterization of the mouse CMP *in vivo* and demonstrates that Muc5b$^{-/-}$ mice harbor a porous CMP that enables pathogens to ascend from the vagina into the uterus. This promotes immune cell infiltration and inflammatory cytokine production, which lead to preterm labor. This work highlights the crucial *in vivo* role of mucus as a physical barrier and of Muc5b in the defense of the uterine cavity against pathogens during pregnancy.

Limitations of the study

The mouse proved to be a model of choice for our study, but the size of the mouse cervical canal and the very small volume of mucus in the CMP are limitations of the model. The limited amount of mucus does not allow for rheology studies. The porosity of the mucus was therefore only studied by imaging. Quantification of both mouse Muc5b and Muc5ac at the peptide level appears to be difficult to achieve. Immunofluorescence imaging gave an indication but no quantitative information. Expression of the corresponding genes was performed by RT-qPCR, but this may not reflect mucin production.

We have demonstrated that Muc5b-deficient CMP is responsible for a high risk of prematurity after vaginal infection. However, our results were obtained in a mouse model and remain to be confirmed in pregnant women carrying the *MUC5B* or *MUC5AC* gene with a nonsense or missense mutation.

STAR★METHODS

Detailed methods are provided in the online version of this paper and include the following:

- KEY RESOURCES TABLE
- RESOURCE AVAILABILITY
  - Lead contact
  - Materials availability
  - Data and code availability
- EXPERIMENTAL MODEL AND SUBJECT DETAILS
  - Mice and generation of timed pregnant mice
- METHOD DETAILS
  - Tissue collection
  - RT-qPCR
  - Bacterial strain and culture conditions
  - Vaginal infection
  - Histology and IHC
  - Thickness of the mucosal epithelium and nonmucosal epithelium
  - Determination of the porosity of CMPs
  - SEM
  - TUNEL
  - iDISCO
  - ELISA
- QUANTIFICATION AND STATISTICAL ANALYSIS

SUPPLEMENTAL INFORMATION

Supplemental information can be found online at https://doi.org/10.1016/j.isci.2022.104526.

ACKNOWLEDGMENTS

We thank J. Devassine (Animal Core Facility, UMS 2014 – US 41 – PLBS/Plateformes Lilloise en Biologie et Santé) and M-H. Gevaert (UMS 2014 – US 41 – PLBS) for the histological sections, M. Tardivel and A. Bongiovanni for cell imaging (BICeL, UMS 2014 – US 41 – PLBS), N. Barois for electron microscopy (BICeL, UMS 2014 – US 41 – PLBS), and S. Plet (Inserm U1286) for technical support. The 45M1, anti-TFF3, and Eu1/Eu2 antibodies were kindly given by J. Bara, C. Tomasetto (IGBMC, Université de Strasbourg, France), and D. Swallow, respectively. This work was supported by the « 1000 days for health » program (FHU from Univ. Lille, France) and the University of Lille, France (GL PhD fellowship).

AUTHOR CONTRIBUTIONS

Conceptualization, G.L., V.G., and J-L.D.; Experiments, G.L., V.G., and M.R.; Analysis, G.L., V.G., M.R., and J-L.D.; Writing, G.L., V.G., and J-L.D.; Review & Editing, All authors.

DECLARATION OF INTERESTS

The authors declare no competing interests.

Received: December 18, 2021
Revised: March 14, 2022
Accepted: May 29, 2022
Published: July 15, 2022

REFERENCES

Amini, S.-E., Gouyer, V., Portal, C., Gottrand, F., and Desseyn, J.-L. (2019). Muc5b is mainly expressed and sialylated in the nasal olfactory epithelium whereas Muc5ac is exclusively expressed and fucosylated in the nasal respiratory epithelium. Histochem. Cell Biol. *152*, 167–174. https://doi.org/10.1007/s00418-019-01785-5.

Bastholm, S.K., Becher, N., Stubbe, P.R., Chronakis, I.S., and Uldbjerg, N. (2014). The viscoelastic properties of the cervical mucus plug. Acta Obstet. Gynecol. Scand. *93*, 201–208. https://doi.org/10.1111/aogs.12308.

Bastholm, S.K., Samson, M.H., Becher, N., Hansen, L.K., Stubbe, P.R., Chronakis, I.S., Nexo, E., and Uldbjerg, N. (2017). Trefoil factor peptide 3 is positively correlated with the viscoelastic properties of the cervical mucus plug. Acta Obstet. Gynecol. Scand. *96*, 47–52. https://doi.org/10.1111/aogs.13038.

Belle, M., Godefroy, D., Couly, G., Malone, S.A., Collier, F., Giacobini, P., and Chédotal, A. (2017). Tridimensional visualization and analysis of early human development. Cell *169*, 161–173.e12. https://doi.org/10.1016/j.cell.2017.03.008.

Belle, M., Godefroy, D., Dominici, C., Heitz-Marchaland, C., Zelina, P., Hellal, F., Bradke, F., and Chédotal, A. (2014). A simple method for 3D analysis of immunolabeled axonal tracts in a transparent nervous system. Cell Rep. *9*, 1191–1201. https://doi.org/10.1016/j.celrep.2014.10.037.

Byers, S.L., Wiles, M.V., Dunn, S.L., and Taft, R.A. (2012). Mouse estrous cycle identification tool and images. PLoS One *7*, e35538. https://doi.org/10.1371/journal.pone.0035538.

Carretero, A., Ruberte, J., and Navarro, M. (2017). 9 - female genital organs. In Morphological Mouse Phenotyping, J. Ruberte, A. Carretero, and M. Navarro, eds. (Academic Press), pp. 227–251. https://doi.org/10.1016/B978-0-12-812972-2.50009-X.

Critchfield, A.S., Yao, G., Jaishankar, A., Friedlander, R.S., Lieleg, O., Doyle, P.S., McKinley, G., House, M., and Ribbeck, K. (2013). Cervical mucus properties stratify risk for preterm birth. PLoS One *8*, e69528. https://doi.org/10.1371/journal.pone.0069528.

Demouveaux, B., Gouyer, V., Gottrand, F., Narita, T., and Desseyn, J.-L. (2018). Gel-forming mucin interactome drives mucus viscoelasticity. Adv. Colloid Interface Sci. *252*, 69–82. https://doi.org/10.1016/j.cis.2017.12.005.

Desseyn, J.-L., and Laine, A. (2003). Characterization of mouse muc6 and evidence of conservation of the gel-forming mucin gene cluster between human and mouse. Genomics *81*, 433–436. https://doi.org/10.1016/s0888-7543(03)00036-3.

Dickinson, J.D., Sweeter, J.M., Staab, E.B., Nelson, A.J., Bailey, K.L., Warren, K.J., Jaramillo, A.M., Dickey, B.F., and Poole, J.A. (2019). MyD88 controls airway epithelial Muc5ac expression during TLR activation conditions from agricultural organic dust exposure. Am. J. Physiol. Lung Cell Mol. Physiol. *316*, L334–L347. https://doi.org/10.1152/ajplung.00206.2018.

Ermund, A., Meiss, L.N., Rodriguez-Pineiro, A.M., Bähr, A., Nilsson, H.E., Trillo-Muyo, S., Ridley, C., Thornton, D.J., Wine, J.J., Hebert, H., et al. (2017). The normal trachea is cleaned by MUC5B mucin bundles from the submucosal glands coated with the MUC5AC mucin. Biochem. Biophys. Res. Commun. *492*, 331–337. https://doi.org/10.1016/j.bbrc.2017.08.113.

Gipson, I.K., Ho, S.B., Spurr-Michaud, S.J., Tisdale, A.S., Zhan, Q., Torlakovic, E., Pudney, J., Anderson, D.J., Toribara, N.W., and Hill, J.A., III (1997). Mucin genes expressed by human female reproductive tract Epithelia1. Biol. Reprod. *56*, 999–1011. https://doi.org/10.1095/biolreprod56.4.999.

Gipson, I.K., Moccia, R., Spurr-Michaud, S., Argüeso, P., Gargiulo, A.R., Hill, J.A., III, Offner, G.D., and Keutmann, H.T. (2001). The amount of MUC5B mucin in cervical mucus peaks at Midcycle. J. Clin. Endocrinol. Metab. *86*, 594–600. https://doi.org/10.1210/jcem.86.2.7174.

Gouyer, V., Demouveaux, B., Lacroix, G., Valque, H., Gottrand, F., and Desseyn, J.-L. (2018). Non-C-mannosylable mucin CYS domains hindered proper folding and secretion of mucin. Biochem. Biophys. Res. Commun. *506*, 812–818. https://doi.org/10.1016/j.bbrc.2018.10.138.

Gouyer, V., Dubuquoy, L., Robbe-Masselot, C., Neut, C., Singer, E., Plet, S., Geboes, K., Desreumaux, P., Gottrand, F., and Desseyn, J.-L. (2015). Delivery of a mucin domain enriched in cysteine residues strengthens the intestinal mucous barrier. Sci. Rep. *5*, 9577. https://doi.org/10.1038/srep09577.

Gouyer, V., Gottrand, F., and Desseyn, J.-L. (2011). The extraordinarily complex but highly structured organization of intestinal mucus-gel unveiled in multicolor images. PLoS One *6*, e18761. https://doi.org/10.1371/journal.pone.0018761.

Gouyer, V., Leir, S.-H., Tetaert, D., Liu, Y., Gottrand, F., Harris, A., and Desseyn, J.-L. (2010). The characterization of the first anti-mouse Muc6 antibody shows an increased expression of the mucin in pancreatic tissue of Cftr-knockout mice. Histochem. Cell Biol. *133*, 517–525. https://doi.org/10.1007/s00418-010-0688-8.

Habte, H.H., de Beer, C., Lotz, Z.E., Tyler, M.G., Schoeman, L., Kahn, D., and Mall, A.S. (2008). The inhibition of the Human Immunodeficiency Virus type 1 activity by crude and purified human pregnancy plug mucus and mucins in an inhibition assay. Virol. J. *5*, 59. https://doi.org/10.1186/1743-422X-5-59.

Han, L., Park, D., Reddy, A., Wilmarth, P.A., and Jensen, J.T. (2021). Comparing endocervical mucus proteome of humans and rhesus macaques. Proteomics Clin. Appl. *15*, e2100023. https://doi.org/10.1002/prca.202100023.

Hein, M., Petersen, A.C., Helmig, R.B., Uldbjerg, N., and Reinholdt, J. (2005). Immunoglobulin levels and phagocytes in the cervical mucus plug at term of pregnancy. Acta Obstet. Gynecol. Scand. *84*, 734–742. https://doi.org/10.1111/j.0001-6349.2005.00525.x.

Karam, S.M., Tomasetto, C., and Rio, M.-C. (2004). Trefoil factor 1 is required for the commitment programme of mouse oxyntic epithelial progenitors. Gut *53*, 1408–1415. https://doi.org/10.1136/gut.2003.031963.

Lacroix, G., Gouyer, V., Gottrand, F., and Desseyn, J.-L. (2020). The cervicovaginal mucus barrier. Int. J. Mol. Sci. *21*, 8266. https://doi.org/10.3390/ijms21218266.

Lee, D.-C., Hassan, S.S., Romero, R., Tarca, A.L., Bhatti, G., Gervasi, M.T., Caruso, J.A., Stemmer, P.M., Kim, C.J., Hansen, L.K., et al. (2011). Protein profiling underscores immunological functions of uterine cervical mucus plug in human pregnancy. J. Proteomics *74*, 817–828. https://doi.org/10.1016/j.jprot.2011.02.025.

Liu, L., Oza, S., Hogan, D., Perin, J., Rudan, I., Lawn, J.E., Cousens, S., Mathers, C., and Black, R.E. (2015). Global, regional, and national causes of child mortality in 2000-13, with projections to inform post-2015 priorities: an updated systematic analysis. Lancet *385*, 430–440. https://doi.org/10.1016/S0140-6736(14)61698-6.

Loux, S.C., Scoggin, K.E., Troedsson, M.H.T., Squires, E.L., and Ball, B.A. (2017). Characterization of the cervical mucus plug in mares. Reproduction *153*, 197–210. https://doi.org/10.1530/REP-16-0396.

Madsen, J., Nielsen, O., Tornøe, I., Thim, L., and Holmskov, U. (2007). Tissue localization of human trefoil factors 1, 2, and 3. J. Histochem. Cytochem. *55*, 505–513. https://doi.org/10.1369/jhc.6a7100.2007.

Matsuo, K., Ota, H., Akamatsu, T., Sugiyama, A., Katsuyama, T., and SugiyAmA, A. (1997). Histochemistry of the surface mucous gel layer of the human colon. Gut *40*, 782–789. https://doi.org/10.1136/gut.40.6.782.

McDonald, H.M., O'Loughlin, J.A., Jolley, P., Vigneswaran, R., and McDonald, P.J. (1991). Vaginal infection and preterm labour. Br. J. Obstet. Gynaecol. *98*, 427–435. https://doi.org/10.1111/j.1471-0528.1991.tb10335.x.

Mendz, G.L., Kaakoush, N.O., and Quinlivan, J.A. (2013). Bacterial aetiological agents of

intra-amniotic infections and preterm birth in pregnant women. Front. Cell. Infect. Microbiol. *3*, 58. https://doi.org/10.3389/fcimb.2013.00058.

Migale, R., Herbert, B.R., Lee, Y.S., Sykes, L., Waddington, S.N., Peebles, D., Hagberg, H., Johnson, M.R., Bennett, P.R., and MacIntyre, D.A. (2015). Specific lipopolysaccharide serotypes induce differential maternal and neonatal inflammatory responses in a murine model of preterm labor. Am. J. Pathol. *185*, 2390–2401. https://doi.org/10.1016/j.ajpath.2015.05.015.

Muzny, C.A., Taylor, C.M., Swords, W.E., Tamhane, A., Chattopadhyay, D., Cerca, N., and Schwebke, J.R. (2019). An updated conceptual model on the pathogenesis of bacterial vaginosis. J. Infect. Dis. *220*, 1399–1405. https://doi.org/10.1093/infdis/jiz342.

Owiny, J.R., Fitzpatrick, R.J., Spiller, D.G., and Dobson, H. (1991). Mechanical properties of the ovine cervix during pregnancy, labour and immediately after parturition. Br. Vet. J. *147*, 432–436. https://doi.org/10.1016/0007-1935(91)90085-2.

Pavlidis, I., Spiller, O.B., Sammut Demarco, G., MacPherson, H., Howie, S.E.M., Norman, J.E., and Stock, S.J. (2020). Cervical epithelial damage promotes Ureaplasma parvum ascending infection, intrauterine inflammation and preterm birth induction in mice. Nat. Commun. *11*, 199. https://doi.org/10.1038/s41467-019-14089-y.

Platt, M.J. (2014). Outcomes in preterm infants. Publ. Health *128*, 399–403. https://doi.org/10.1016/j.puhe.2014.03.010.

Portal, C., Gouyer, V., Gottrand, F., and Desseyn, J.-L. (2017a). Preclinical mouse model to monitor live Muc5b-producing conjunctival goblet cell density under pharmacological treatments. PLoS One *12*, e0174764. https://doi.org/10.1371/journal.pone.0174764.

Portal, C., Gouyer, V., Magnien, M., Plet, S., Gottrand, F., and Desseyn, J.-L. (2017b). In vivo imaging of the Muc5b gel-forming mucin. Sci. Rep. *7*, e44591. https://doi.org/10.1038/srep44591.

Ream, M.A., and Lehwald, L. (2018). Neurologic consequences of preterm birth. Curr. Neurol. Neurosci. Rep. *18*, 48. https://doi.org/10.1007/s11910-018-0862-2.

Rousseau, K., Wickstrom, C., Whitehouse, D.B., Carlstedt, I., and Swallow, D.M. (2003). New monoclonal antibodies to non-glycosylated domains of the secreted mucins MUC5B and MUC7. Hybrid. Hybridomics *22*, 293–299. https://doi.org/10.1089/153685903322538818.

Sierra, L.-J., Brown, A.G., Barilá, G.O., Anton, L., Barnum, C.E., Shetye, S.S., Soslowsky, L.J., and Elovitz, M.A. (2018). Colonization of the cervicovaginal space with Gardnerella vaginalis leads to local inflammation and cervical remodeling in pregnant mice. PLoS One *13*, e0191524. https://doi.org/10.1371/journal.pone.0191524.

Smith-Dupont, K.B., Wagner, C.E., Witten, J., Conroy, K., Rudoltz, H., Pagidas, K., Snegovskikh, V., House, M., and Ribbeck, K. (2017). Probing the potential of mucus permeability to signify preterm birth risk. Sci. Rep. *7*, 10302. https://doi.org/10.1038/s41598-017-08057-z.

Sperling, L.S., and Nelson, J.R. (2016). History and future of omega-3 fatty acids in cardiovascular disease. Curr. Med. Res. Opin. *32*, 301–311. https://doi.org/10.1185/03007995.2015.1120190.

Stinson, L.F., and Payne, M.S. (2019). Infection-mediated preterm birth: bacterial origins and avenues for intervention. Aust. N. Z. J. Obstet. Gynaecol. *59*, 781–790. https://doi.org/10.1111/ajo.13078.

Suff, N., Karda, R., Diaz, J.A., Ng, J., Baruteau, J., Perocheau, D., Tangney, M., Taylor, P.W., Peebles, D., Buckley, S.M.K., and Waddington, S.N. (2018). Ascending vaginal infection using bioluminescent bacteria evokes intrauterine inflammation, preterm birth, and neonatal brain injury in pregnant mice. Am. J. Pathol. *188*, 2164–2176. https://doi.org/10.1016/j.ajpath.2018.06.016.

Sugiyama, M., Machida, N., Yasunaga, A., Terai, N., Fukasawa, H., Ono, H.K., Kobayashi, R., Nishiyama, K., Hashimoto, O., Kurusu, S., and Yoshioka, K. (2021). Vaginal mucus in mice: developmental and gene expression features of epithelial mucous cells during pregnancy. Biol. Reprod. *105*, 1272–1282. https://doi.org/10.1093/biolre/ioab157.

Tetaert, D., Pierre, M., Demeyer, D., Husson, M.-O., Béghin, L., Galabert, C., Gottrand, F., Beermann, C., Guery, B., and Desseyn, J.-L. (2007). Dietary n-3 fatty acids have suppressive effects on mucin upregulation in mice infected with Pseudomonas aeruginosa. Respir. Res. *8*, 39. https://doi.org/10.1186/1465-9921-8-39.

Valque, H., Gouyer, V., Gottrand, F., and Desseyn, J.-L. (2012). MUC5B leads to aggressive behavior of breast cancer MCF7 cells. PLoS One *7*, e46699. https://doi.org/10.1371/journal.pone.0046699.

Valque, H., Gouyer, V., Husson, M.-O., Gottrand, F., and Desseyn, J.-L. (2011). Abnormal expression of Muc5b in Cftr-null mice and in mammary tumors of MMTV-ras mice. Histochem. Cell Biol. *136*, 699–708. https://doi.org/10.1007/s00418-011-0872-5.

Velíšek, L. (2016). Under the (light) sheet after the iDISCO+. Epilepsy Curr. *16*, 405–407. https://doi.org/10.5698/1535-7511-16.6.405.

Wickström, C., Davies, J.R., Eriksen, G.V., Veerman, E.C.I., and Carlstedt, I. (1998). MUC5B is a major gel-forming, oligomeric mucin from human salivary gland, respiratory tract and endocervix: identification of glycoforms and C-terminal cleavage. Biochem. J. *334*, 685–693. https://doi.org/10.1042/bj3340685.

STAR★METHODS

KEY RESOURCES TABLE

REAGENT or RESOURCE	SOURCE	IDENTIFIER
Antibodies		
Monoclonal anti-MUC5AC	Gift from J. Bara	45M1
Polyclonal anti-Muc5b	Valque et al., 2011	CP1
Polyclonal anti-Muc6	Gouyer et al., 2010	CP4
Polyclonal anti-MUC2	Novus Biologicals	Cat# NBP1-31231; RRID: AB_10003763
Monoclonal anti-MUC5AC	Rousseau et al., 2003	EU1/EU2
Polyclonal anti-GFP	Abcam	Ab290; RRID: AB_303395
Tff3/TFF3	Karam et al., 2004	anti-TFF3 antibody
Anti-*Escherichia coli*	VWR	Cat# USBIE3500-06J; RRID: AB_10775996
Monoclonal anti-PCNA	Abcam	PC10 Ab29; RRID AB_303394
Fluorescein (FITC) AffiniPure F(ab')$_2$ Fragment Goat Anti-Rabbit IgG, F(ab')$_2$ fragment specific	Jackson	Cat# 111-096-047; RRID: AB_2337982
Fluorescein (FITC) AffiniPure F(ab')$_2$ Fragment Rabbit Anti-Goat IgG, F(ab')$_2$ fragment specific	Jackson	Cat# 305-096-006; RRID: AB_2339446
Fluorescein (FITC) AffiniPure Goat Anti-Mouse IgG, F(ab')$_2$ fragment specific	Jackson	Cat# 115-095-006; RRID: AB_2338590
Rhodamine (TRITC) AffiniPure Rabbit Anti-Mouse IgG, F(ab')$_2$ fragment specific	Jackson	Cat# 315-025-006; RRID: AB_2340049
Bacterial and virus strains		
Gardnerella vaginalis	Institut Pasteur Collection	CIP 70.74T
Escherichia coli serotype O55:K59(B5):H–	ATCC	CDC 5624-50 [NCTC 9701]
Chemicals, peptides, and recombinant proteins		
PBS	Gibco, Life Technologies, France	Cat# 12559069
Xylene	Sigma-Aldrich	Cat# 1330-20-7
Ethanol	Carlo Erba	Cat# 64-17-5
Petroleum jelly	Laboratoire Gilbert	
Ketamine	Virbac	
Xylazine	Dechra, France	
Prechilled tubes containing EDTA	Vacuette tubes, France	
RNAlater	Invitrogen	Cat# AM7020
gelatin	Sigma-Aldrich	Cat# 9000-70-8
Tween	Sigma-Aldrich	Cat# 9005-64-5
Triton X-100	Sigma-Aldrich	Cat# 9036-19-5
Saponin	Sigma-Aldrich	Cat# 8047-15-2
Sodium azide	Research Organics Inc., OH	Cat# 0939S
Acetic acid	Carlo Erba	Cat# 64-19-7
Chloroform	Carlo Erba	Cat# 67-66-3
Methanol	Carlo Erba	Cat# 67-56-1
Dichloromethane	Sigma-Aldrich, USA	Cat# 75-09-2
Hydrogen peroxide	Sigma-Aldrich	Cat# 7722-84-1
Dibenzylether	Sigma-Aldrich	Cat# 103-50-4
Trisodium citrate dihydrate	Sigma-Aldrich	Cat# 6132-04-3

(*Continued on next page*)

Continued

REAGENT or RESOURCE	SOURCE	IDENTIFIER
Critical commercial assays		
In Situ Cell Death Detection Kit, Fluorescein	Roche	Cat# 11684795910
BCA Protein Assay kit	Pierce BCA, Thermo Scientific	Cat# 10741395
ELISA mouse Il-1®	Invitrogen	Cat# 88-7013-22
ELISA mouse CXCL1/KC	R&D Systems	Cat# DY453-05
ELISA mouse Il-6 250X capture antibody	eBioscience, Thermo Scientific	Cat# 14-7061-68
ELISA mouse Il-6 250X detection antibody	eBioscience, Thermo Scientific	Cat# 13-7062-68A
ELISA mouse Il-10 250X capture antibody	eBioscience, Thermo Scientific	Cat# 14-7102-68
ELISA mouse Il-10 250X detection antibody	eBioscience, Thermo Scientific	Cat# 13-7101-68
ELISA mouse Tnf-α capture antibody	eBioscience, Thermo Scientific	Cat# 14-7423-68A
ELISA mouse Tnf-α detection antibody	eBioscience, Thermo Scientific	Cat# 13-7341-68A
Universal PCR Master Mix	Applied Biosystems	Cat# 10733457
Rnasin RNase inhibitor	Promega	Cat# N251B
M-MuLV Reverse Transcriptase	New England Biolabs	Cat# 50-811-670
M-MuLV Reverse Transcriptase Reaction Buffer	New England Biolabs	Cat# B0253S
Random hexamer	Invitrogen	Cat# 100026484
TaqMan™ Ribosomal RNA Control Reagents	Applied Biosystems	Cat# 4308329
Experimental models: Organisms/strains		
Mouse: Muc5b-GFP: C57BL/6	In house	N/A
Mouse: Muc5b knockout: C57BL/6	In house	N/A
Mouse: Tff3-GFP: C57BL/6	In house	Tg222
Mouse: Control WT C57BL/6	In house	N/A
Oligonucleotides		
CHOP (fwd) GAATAACAGCCGGAACCTGA	This paper	N/A
CHOP (rev) TCAGGTGTGGTGGTGTATGAA	This paper	N/A
CHOP (TaqMan probe) GGAGAGAGTGTTCAAGAAGGAAGTGTA	Gouyer et al., 2018	N/A
Software and algorithms		
Fiji	https://imagej.net/software/fiji/	Version 1.53k
ZEN software	Zeiss	Version 2.5.75.0
ImspectorPro	LaVision BioTec	Version 3.6.3
ImspectorfileConverter	LaVision BioTec	Version 9.8.0
Imaris x64	Imaris Oxford	Version 9.8.0, Bitplane
StatXact	Cytel Studio	Version 6.0
Other		
TRITC Conjugated *Ulex europaeus* Lectin (Gorse, Furze)–UEA-I– 2mg	EY Laboratories	Cat# R-2202-2
TRITC Conjugated *Maackia amurensis* Lectin –MAA– 2mg	EY Laboratories	Cat# R-7801-2
LB Broth	Sigma	Cat# L3522
LB Broth with agar	Sigma	Cat# L2897
Mueller Hinton broth	Oxoid	Cat# CM0405
Mueller Hinton agar	Oxoid	Cat# CM0337B
Horse blood defibrinated	Thermo Scientific	Cat# 10200013

RESOURCE AVAILABILITY

Lead contact

Further information and requests for resources and reagents should be directed to the lead contact, Dr. Jean-Luc Desseyn (jean-luc.desseyn@inserm.fr).

Materials availability

- This study did not generate new unique reagents or mouse lines.
- Non commercial antibodies are available from lead contact upon request.

Data and code availability

- All data produced in this study are included in the published article and its supplemental information, or are available from the lead contact upon request.
- This paper does not report original code.
- Any additional information required to reanalyze the data reported in this paper is available from the lead contact upon request.

EXPERIMENTAL MODEL AND SUBJECT DETAILS

Mice and generation of timed pregnant mice

Mice were housed under standard conditions in a specific pathogen-free animal facility and received a standard chow diet *ad libitum*. The methods used in all animal studies were carried out in accordance with the French Guidelines for the Care and Use of Laboratory Animals and with the guidelines of the European Union. All experimental protocols for animal experiments were approved by the regional Institutional Animal Care Committee (approvals: APAFIS#8204–2016120914269637). Eight to 16-week-old C57BL/6 WT mice, Muc5b-GFP, Muc5b$^{-/-}$, and Tg222 transgenic mice with the C57BL/6 genetic background were used (Amini et al., 2019; Gouyer et al., 2015; Portal et al., 2017b). For timed breeding, the stage of the estrous cycle was identified by the presence, absence or proportional numbers of cornified epithelial cells, nucleated epithelial cells and leukocytes in vaginal smears. Only cornified epithelial cells are observed in vaginal smears at estrus (ovulation) (Byers et al., 2012). Each female was paired with one adult male for one night. The day after mating was considered GD0.5.

METHOD DETAILS

Tissue collection

Mice were killed by cervical dislocation. Expression of GFMs during the estrus cycle was examined in 6–12 weeks-old WT mice. The phase of the estrous cycle was determined by histology according to a previous report (Carretero et al., 2017). Vaginas, cervices, and part of the uterine horns were collected as a single continuous tissue and rinsed in phosphate-buffered saline (PBS). To assess inflammation, the proximal uterus was collected. Tissues were immediately placed in fresh Carnoy's fixative solution (60% ethanol, 30% acetic acid, 10% chloroform) for 5 h, stored in 70% ethanol, and embedded in paraffin for histological studies or in PBS with 0.01% sodium azide at +4°C for iDISCO. Tissues for RT-qPCR were placed directly in RNAlater for 24 h and then stored at −80°C until use.

RT-qPCR

Real-time TaqMan probe-based RT-qPCR was performed as follows. Total RNA from the vagina/cervix was extracted using 1.5 mL TRI Reagent following the manufacturer's protocol. Reverse transcription was performed with 2 μg of RNA using random hexamers and 0.2 U of MMLV Reverse Transcriptase (Portal et al., 2017a). The oligonucleotides and probes used to measure *Muc5b*, *Muc5ac*, *Muc2*, and *Muc6* expression have been published (Gouyer et al., 2010, 2015; Tetaert et al., 2007). Endoplasmic reticulum stress was evaluated by identifying upregulation of CHOP by RT-qPCR. The specific primers were designed as previously described for *Macaca* CHOP with the *Macaca* internal TaqMan probe overlapping the exon 1–exon 2 junction and conserved in mice (Gouyer et al., 2018). Duplex PCR amplification was carried out in 25 μL reaction volume containing 2 μL of the first strand cDNA, 10 pmol of each primer for a given mucin studied, 5 pmol of mucin probe and TaqMan Universal PCR Master Mix 2X (Applied Biosystems) containing 1 pmol of the

18S-primers (sense and antisense), 5 pmol of the 18S-probe (5′ Vic reporter dye), 5,6-carboxy-x-rhodamine (ROX), the Taq DNA polymerase and the requisite buffers (Tetaert et al., 2007). All amplifications were performed in triplicate using a QuantStudio 3 Real-Time PCR System and 18S rRNA as an internal control. For each sample, the ratio of amplification was calculated as $2^{-(\text{Ctmean, target gene} - \text{Ctmean, 18S rRNA})}$.

Bacterial strain and culture conditions

Gardnerella vaginalis was grown in Oxoid Mueller–Hinton medium with 5% defibrinated horse blood at 37°C in an atmosphere enriched with carbon dioxide (CO_2 gas generator, BD Diagnostics, France). *Escherichia coli* serotype O55:K59(B5):H– was grown aerobically with shaking at 37°C in Luria–Bertani medium.

Vaginal infection

Experimental vaginal infection was induced in an animal biosafety level 2 facility at the University of Lille, France. Two to 6-month-old female mice were time mated as previously described. Twenty microliters of midlogarithmic-phase bacteria (5×10^8 and 5×10^7 CFU/mL of *G. vaginalis* and *E. coli* O 55, respectively) resuspended in PBS were inoculated into the vagina at GD14.5 using a 200 μL pipette tip. Immediately after the inoculation, petroleum jelly was added with a sterile swab to ensure the inoculum remained within the cervicovaginal space. To confirm the dose of bacteria administrated, the CFUs were determined systematically by serial dilutions of bacteria and cultured in agar plates. One or two days before the vaginal infection, mice were transferred to individual cages and observed twice a day for signs of preterm birth. Preterm delivery was determined as birth occurring before GD18.5.

Once delivery had occurred, blood samples were collected from six mice per genotype into prechilled tubes containing EDTA by cardiac puncture immediately after induction of anesthesia with ketamine–xylazine (2v/1v). Serum was collected by centrifugation at 10,000 *g* for 10 min and stored at −80°C for measurement of cytokine concentration using ELISAs. The part of the uterine tissue facing the cervical canal was collected and stored at −80°C for ELISA analysis.

Ascending vaginal infection was analyzed 24 h after infection in three WT and three $Muc5b^{-/-}$ pregnant mice. The vaginas/cervices were collected for histology and IHC.

Histology and IHC

Longitudinal 5-μm-thick sections of paraffin tissue were cut. Histological studies using either HE or AB–PAS staining and IHC studies using anti-Muc5ac, Muc5b, Muc2 and Muc6 antibodies were performed as follows. Paraffin sections were dewaxed with xylene and rehydrated through decreasing ethanol washes. The tissue sections were blocked with 1% bovine serum albumin (BSA) in PBS for 45 min and incubated with anti-Muc5ac (1:500), anti-Muc5b (1:50), anti-Muc6 (1:50), or anti-Muc2 (1:100) diluted in PBS/1% BSA overnight at 4°C. The slides were washed three times in PBS, incubated for 2 h with FITC-conjugated secondary antibodies (1:150) diluted in PBS/1% BSA, and rinsed in PBS. Nuclei were counterstained with Hoechst 33258 solution (1:1000) for 5 min. The immunolabeled sections were dried and mounted with Mowiol Mounting Medium (Gouyer et al., 2010; Valque et al., 2011). Tissue sections of the mouse genital tract were also stained with a commercial Muc2 antibody. The transgene product of the Tg222 mouse was labeled using antibodies Eu1/Eu2 directed against the human MUC5B CYS domain as described earlier (Gouyer et al., 2015; Valque et al., 2012). Anti-TFF3 antibody crossreacting with the mouse Tff3 was used at 1:100 (Karam et al., 2004). Commercial anti-GFP antibody was used at 1:500 to label Muc5b–GFP (Gouyer et al., 2015; Portal et al., 2017a). Anti-*E. coli* labeling was performed using the primary goat anti-*E. coli* serotype O antibody (1:1000). PCNA was studied using the PC10 anti-PCNA monoclonal antibody (1:1000). For Muc5ac, Muc2, GFP, Tff3 and PCNA immunolabeling, the sections were pretreated using sodium citrate buffer (10mM tri-sodium citrate, 0.05% tween, pH6) at 95°C for 20 min and then at room temperature for 20 min (Gouyer et al., 2010). Fluorescein isothiocyanate (FITC)-conjugated anti-rabbit-IgG, anti-goat-IgG, and anti-mouse-IgG secondary antibodies were used. For GFP and Muc5ac double labeling, FITC-conjugated anti-rabbit-IgG and tetramethyl rhodamine isothiocyanate (TRITC)-conjugated anti-mouse-IgG secondary antibodies were used. TRITC-conjugated UEA1 and *Maackia amurensis* agglutinin lectins were used at 25 μg/mL (Gouyer et al., 2015). Nuclei were counterstained with Hoechst 33258 (1:1000).

Histology and IHC were performed on a Leica DM4000B microscope. High-quality bright field and fluorescence captures were digitized on a Carl Zeiss Axio Scan Z1 scanner and processed with ZEN software. Image analysis was performed using ImageJ/Fiji freeware. The total number of epithelial cells and $PCNA^+$ epithelial cells in the vagina and cervix were counted for 3–6 distinct sections per mouse (n3/genotype) in a blinded manner by two independent observers (GL and VG). The number of $PCNA^+$ cells was expressed as the total number of $PCNA^+$ cells per 100 epithelial cells.

Thickness of the mucosal epithelium and nonmucosal epithelium

The thickness of ME and nonmucosal epithelium (NME, defined as the epithelium with no visible mucus-laden vacuoles) was measured as follows: 20–40 measurements of the ME and NME were performed for each field using ImageJ. Data were obtained using at least three AB–PAS-stained sections of vagina per mouse. Four mice per genotype were analyzed to ensure accurate results.

Determination of the porosity of CMPs

The mean CMP porosity was calculated using ImageJ analysis as follows. AB–PAS-stained images were converted to eight-bit intensity images with a grayscale color map. Pixel segmentation was then undertaken by converting the absence and presence of glycoconjugates to red and gray, respectively. Porosity was calculated as the sum of all areas in red (empty) divided by the total area of the region of interest (ROI), expressed as a percentage. Data were obtained using three distinct ROIs per CMP from at least four mice/genotype to ensure accurate results.

SEM

Cervices were harvested from four WT and four $Muc5b^{-/-}$ mice at GD14.5. The tissues were immersed in Carnoy's fixative solution for 5 h and placed in 70% ethanol. The following steps were performed at the Lille Pasteur Institute. Tissues were postfixed in 70% ethanol supplemented with 1% uranyl acetate at room temperature for 2 h in the dark. The samples were washed in 100% ethanol, air-dried using hexamethyldisilazane, cut in half lengthwise, and mounted on an SEM support with double-sided adhesive carbon tape. Samples were observed with a secondary electron detector in a Zeiss Merlin Compact VP SEM (Zeiss, France) operating at 1 kV. Samples were first observed at low magnification and then at high magnification to characterize the structure of the CMP. Analysis was performed by three independent observers (GL, VG, and JLD), who were unaware of the genotype.

TUNEL

Apoptosis was assessed using the Roche diagnosis TUNEL assay kit. Paraffin-embedded tissues were processed following the manufacturer's specifications using Proteinase K pretreatment. $TUNEL^+$ cells in the vaginal and cervical epithelium were counted in a blinded manner by two independent observers (GL and VG). The total area (μm^2) of the vaginal and cervical epithelium was measured using ImageJ. The results are expressed as the number of $TUNEL^+$ cells per μm^2 of the vaginal or cervical epithelium (n = 5/genotype).

iDISCO

iDISCO was performed as described by Belle et al. (2017) with minor modifications. Bleaching and clearing were performed as described. For immunostaining, primary and secondary antibodies were diluted in 1× PBS containing 0.2% gelatin, 0.5% Triton X-100, and 0.1% saponin. The GFP tag in Muc5b–GFP was immunodetected using anti-GFP antibody. 3D imaging was performed using an ultramicroscope I with ImspectorPro software (Belle et al., 2014). The step size between each image was fixed at 2 μm. Stack images were first converted to an Imaris file (.ims) using ImarisFileConverter. Images, 3D volume, and movies were generated using Imaris ×64 software.

ELISA

Frozen uterus samples were thawed on ice and solubilized in 400 μL ice-cold protein lysis buffer (100 mM DTT, 0.01% NP40) containing protease inhibitors using a Bead Mill 24 homogenizer (4 m/s for 10 s, 10 s dwell time between runs, three times). Total protein concentration was determined using a Pierce BCA Protein Assay kit as per the manufacturer's guidelines and then diluted 1:4 in PBS. All samples were measured in the same assay using ELISA kits for mouse Il-1β, CXCL1/KC, Il-6, Il-10, and Tnf-α according to the manufacturer's guidelines. The cytokine content of tissue homogenates was normalized to protein content and

the data are expressed as pg/μg tissue. Cytokine concentration was determined in 100 μL of pure serum and is expressed as ng/mL.

QUANTIFICATION AND STATISTICAL ANALYSIS

Non-parametric tests were used in all statistical analyses and performed using the statistical StatXact 6.0 package. Two-sided Wilcoxon–Mann–Whitney test was used for all experiments except preterm frequency (Figure 11) where the Barnard's test was used. A p value ≤ 0.05 was considered to be significant.